An Evaluation of the Flammability of 3D Printed Part Parameters Using the Vertical Bunsen Burner Test Method

December 2023

Final report

U.S. Department of Transportation
Federal Aviation Administration

NOTICE

This document is disseminated under the sponsorship of the U.S. Department of Transportation in the interest of information exchange. The U.S. Government assumes no liability for the contents or use thereof. The U.S. Government does not endorse products or manufacturers. Trade or manufacturers' names appear herein solely because they are considered essential to the objective of this report. The findings and conclusions in this report are those of the author(s) and do not necessarily represent the views of the funding agency. This document does not constitute FAA policy. Consult the FAA sponsoring organization listed on the Technical Documentation page as to its use.

This report is available at the Federal Aviation Administration William J. Hughes Technical Center's Full-Text Technical Reports page: actlibrary.tc.faa.gov in Adobe Acrobat portable document format (PDF).

Form DOT F 1700.7 (8-72)   Reproduction of completed page authorized

1. Report No. DOT/FAA/TCTN-23/65	2. Government Accession No.	3. Recipient's Catalog No.
4. Title and Subtitle An Evaluation of the Flammability of 3D Printed Part Parameters Using the Vertical Bunsen Burner Test Method		5. Report Date December 2023
		6. Performing Organization Code
7. Author(s) Dan Keslar, Steven Rehn		8. Performing Organization Report No.
9. Performing Organization Name and Address US Department of Transportation William J. Hughes Technical Center Aviation Research Division Fire Safety Branch, ANG-E21 Atlantic City International Airport, NJ 08405		10. Work Unit No. (TRAIS)
		11. Contract or Grant No.
12. Sponsoring Agency Name and Address Federal Aviation Administration Senior Technical Experts Office (AIR-20) 800 Independence Avenue SW Washington, DC 20591.		13. Type of Report and Period Covered
		14. Sponsoring Agency Code

15. Supplementary Notes

16. Abstract

Additive manufacturing (AM), commonly referred to as three-dimensional (3D) printing, is a modern manufacturing technology that can be applied within many different areas of the aerospace industry due to its ability to produce light and durable parts with complex geometries. Aircraft manufacturers and airlines have expressed interest in the use of AM produced parts in aircraft cabins. However, AM presents new safety challenges that must be examined, including the flammability of the 3D printed part used in the aircraft cabin. Due to the different parameters used during the production process compared to traditional manufacturing methods, it was necessary to determine the effect that variations in print parameters have on the flammability of a 3D printed part. In order to accomplish this, the following print parameters were evaluated; material type, sample thickness (number of inner layers), infill percentage, infill pattern, raster width, raster angle, and print orientation. The scope of this report only includes samples produced from the Fused Filament Fabrication (FFF) AM method, a type of extrusion-based AM process.

Testing was conducted using the Vertical Bunsen Burner (VBB) test methodology outlined in Chapter 1 of the Aircraft Materials Fire Test Handbook (FAA, 2023). In the first phase of testing, only a few variables in the samples were altered and the remaining variables were kept constant so that accurate comparisons between fire data could be made. Subsequently, a Design of Experiments (DOE) analysis was conducted to determine the interaction among multiple print variable combinations.

Results indicate that all evaluated variables had an impact on the flammability of a 3D printed part. The three variables that were observed to have the most significant effect on data were material type, sample thickness, and infill percentage. Other factors such as raster width, raster angle, print orientation, and infill pattern were observed to produce only interaction effects in conjunction with the other print variables listed.

17. Key Words Additive manufacturing, 3D printing, Vertical Bunsen Burner, aircraft materials, infill, raster	18. Distribution Statement This document is available to the U.S. public through the National Technical Information Service (NTIS), Springfield, Virginia 22161. This document is also available from the Federal Aviation Administration William J. Hughes Technical Center at actlibrary.tc.faa.gov.		
19. Security Classif. (of this report) Unclassified	20. Security Classif. (of this page) Unclassified	21. No. of Pages 84	22. Price

Contents

Figures

Tables

Acronyms

Acronym	Definition
3D	3-Dimensional
ABS	Acrylonitrile Butadiene Styrene
AM	Additive Manufacturing
CAGR	Compound Annual Growth Rate
Sparse DD	Sparse Double Dense
DOE	Design of Experiments
FAA	Federal Aviation Administration
FFF	Fused Filament Fabrication
PC	Polycarbonate
PEI	Polyetherimide
PEKK	Polyetherketoneketone
PES	Polyethersulfone
TPES	Total Primary Energy Supply
VBB	Vertical Bunsen Burner

Executive summary

Additive manufacturing (AM), commonly referred to as three-Dimensional (3D) printing, is the process of joining materials, usually layer by layer, to produce an object from a 3D computer model. This technology has seen increased use within the aerospace industry due to the unique advantages it provides compared to traditional manufacturing methods. 3D printed parts have already been utilized in limited instances within the interior of aircraft such as fold down trays and arm chair rests. However, the use of AM produced parts is expected to grow substantially within the near future. New variables present during the AM production process present additional challenges that must be examined to verify that an AM part does not present any greater flammability hazard than a traditionally-manufactured component. Testing is required to determine the effect that alterations in print variables have on the flammability of a 3D printed part.

This study was focused on one particular type of additive manufacturing – Fused Filament Fabrication (FFF) – a type of material extrusion based AM method. Tested samples were manufactured with an on-site FFF machine generated from 3D computer models. Flammability testing was conducted according to the procedures presented within Chapter 1 of the Federal Aviation Administration Aircraft Materials Fire Test Handbook : Vertical Bunsen Burner Test for Cabin and Cargo Compartment Materials , which is one method of showing compliance with 14 CFR 25.853 Fire Protection for Compartment Interiors (Compartment Interiors, 2020). The effects of variations in the following print parameters were evaluated: material, sample thickness (number of inner layers), infill percentage, infill pattern, raster width, raster angle, and print orientation.

Several series of experiments were conducted in which a select few of the parameters were varied and the remaining parameters were kept constant. This allowed for broad comparisons to be made by comparing the flammability test results as parameters were changed. Following these tests, a Design of Experiments (DOE) analysis was conducted to evaluate the interaction effects among different parameter combinations.

Test results indicate that all evaluated parameters had some impact on flammability. The three parameters found to have the largest impact on flammability data were the material type, sample thickness, and infill percentage. Other parameters such as infill pattern, print orientation, raster width, and raster angle were observed to produce only interaction effects in conjunction with the other print variables listed.

1   Introduction

Additive manufacturing (AM), commonly referred as 3D printing, is the process of joining materials, usually layer by layer, to produce an object from a 3D model. AM differs from traditional subtractive manufacturing methods, in that material is added layer by layer to produce a 3D product, whereas in subtractive manufacturing, material is subtracted or removed to create a part. Many different AM types have been developed including material extrusion, powder bed fusion, and binder jetting. However, AM is still a rapidly developing technology so additional methods may be devised in the future. Initially, additive manufacturing was primarily utilized for production of parts used in prototyping or testing. Recently though, AM has seen increased use in the production of final parts intended for end-use.

There is significant interest from the aerospace industry to use AM to produce aircraft cabin components, as AM allows the creation of parts with complex geometries or structures to be designed and produced quickly compared to traditional manufacturing methods. Furthermore, 3D printing allows for the production of lighter and stronger components for aerospace applications (GAO, 2015). This is particularly promising within the aerospace industry, as reductions in weight provide potential for fuel savings, decreases in CO_2 emissions and total primary energy supply (TPES) demands (Joshi & Sheikh, 2015).

AM produced parts have already seen limited use within the interior of aircraft. Examples of this include arm chair rests, video monitor frames, and overhead bin spacer panels, which have all been used within the cabin of aircraft. Figure 1 displays two examples of 3D printed components previously/soon to be installed in aircraft cabins; an overhead bin spacer panel and a video monitor frame used in a Finnair A320 and an Etihad Airways aircraft, respectively (3D printing technology is now taking on airplane interiors, 2017; Molitch-Hou, 2018).
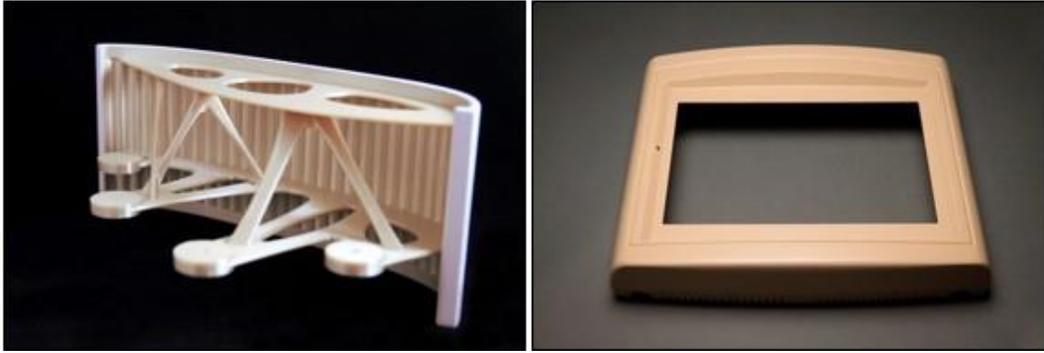
Figure 1. Overheard spacer panel (left) and video monitor frame (right)

Growth in the utilization of 3D printed parts is expected to increase significantly within the near future. The global AM market was valued at 13.8 billion dollars in 2021 and is projected to grow at a compound annual growth rate (CAGR) of 20.8% from 2022 to 2030 (Grand View Research, n.d.). The aerospace industry is expected to be a considerable portion of this market. With this growth, the amount of 3D printed parts utilized within the cabin of aircraft will increase substantially. Therefore, research is needed to verify that an AM part does not present any greater flammability hazard than a traditionally-manufactured component.

A study was conducted to determine the effects of different parameters used in the printing process on a material's flammability. The following parameters were tested; material type, sample thickness (number of inner layers), infill percentage, infill pattern, raster width, raster angle, and print orientation (XY, YZ, ZX). These parameters were defined as follows:

- **Material type**: the substance that the 3D printed part is composed of.

- **Sample thickness (number of inner layers):** the number of inner layers of the test coupon.

- **Infill percentage:** the density of the material inside the 3D printed part, or the amount of material used on the inside of a part divided by the amount of material used if it were solid (Figure 2).
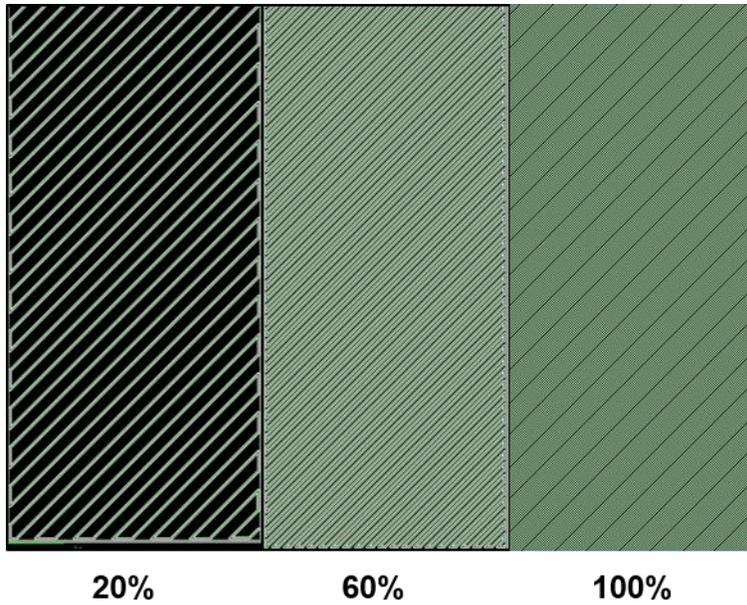
Figure 2. Infill percentage comparisons

- **Infill pattern:** the pattern of the interior of the 3D printed part (Figure 3).
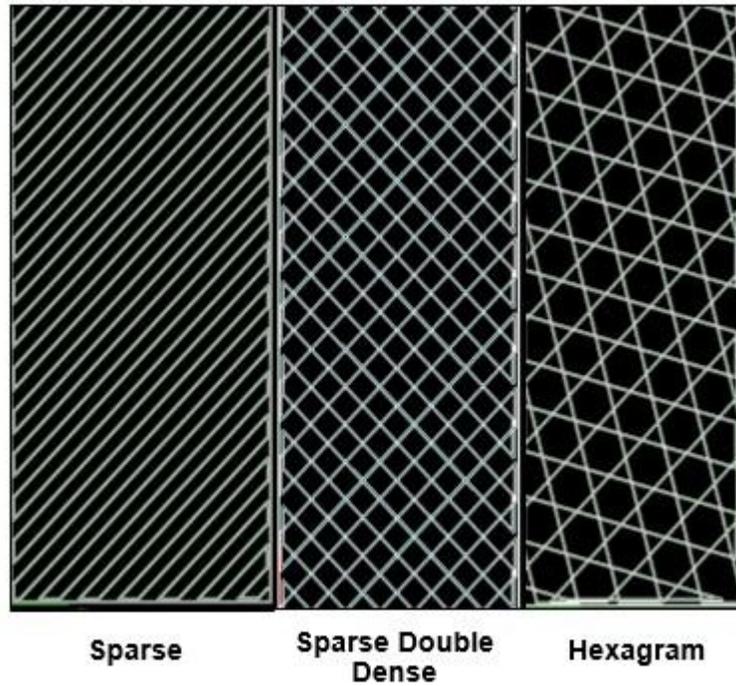
Figure 3. Infill pattern comparisons

- **Raster width:** the width of each extrusion deposited by the nozzle.

- **Raster angle:** the angle between the path of the printing nozzle and the x-axis of the printing platform (Figure 4).

45°   67.5°   90°
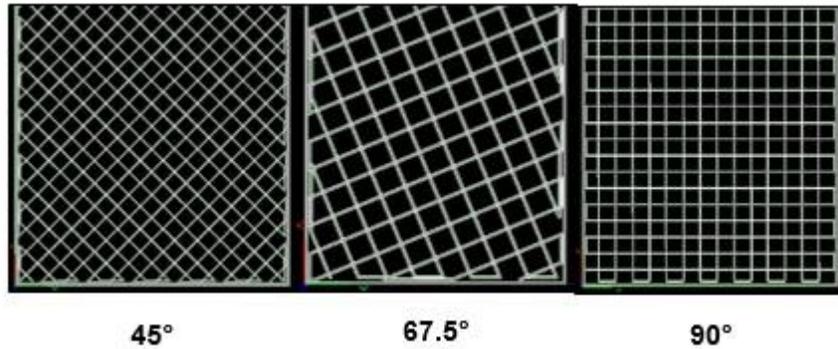
Figure 4. Raster angle comparisons

- **Print orientation**: the inclination of a part on the build platform with respect to the X, Y, and Z axis (Figure 5).
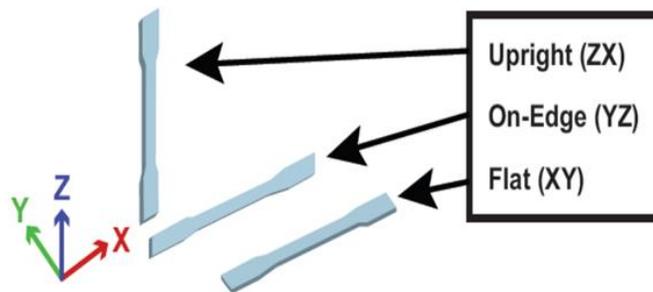
Figure 5. Print orientation comparisons

1.1   Objective

The objective of this study was to determine the impact, if any, that the print parameters of an AM produced part have on the flammability of a sample. The results from this study will be used to develop guidance and help simplify future certification of 3D printed parts. For the scope of this study, only 3D printed samples produced using fused filament fabrication (FFF) were evaluated.

1.2 Experiment procedures

All testing was conducted using the guidelines within the Aircraft Materials Fire Test Handbook (FAA, 2023). Test procedures followed either the 12-second or 60-second Vertical Bunsen Burner (VBB) test method. The burn length, flame time, and drip flame time for each sample was measured and recorded. The definitions of each measurement are as follows, and are displayed visually in Figure 6:

- **Burn length:** the distance from the original specimen edge to the farthest evidence of damage to the test specimen due to that area's combustion, including areas of partial consumption, charring, or embrittlement but not including areas sooted, stained, warped, or discolored, nor areas where material has shrunk or melted away from the heat. This was measured using a ruler to the nearest tenth of an inch.

- **Flame time:** the time in seconds that the specimen continues to flame after the burner flame is removed from beneath the specimen. Surface burning that results in a glow but not in a flame is not included. This was measured using a stopwatch to the nearest tenth of a second.

- **Drip flame time:** the time in seconds that any flaming material continues to flame after falling from the specimen to the floor of the chamber. If no material falls from the specimen, the drip flame time is reported to be 0 seconds, and the notation "No Drip" is also reported. In the event that multiple drips fuel a flame, then the longest continuous flame shall be recorded. This was measured using a stopwatch to the nearest tenth of a second.

All samples throughout this study were created via a Stratasys Fortus 450mc industrial 3D printer. Produced parts from this printer have an achievable accuracy of ± 0.005 inches.

Figure 6. Burn Length, flame time, and drip flame time measurements, respectively

2 Single variable testing

Initial testing was conducted in which individual parameters were isolated and evaluated with the VBB test. In this stage of testing, the flammability impact of the following parameters was evaluated; material type, sample thickness (number of inner layers), infill percentage, infill pattern, raster width, raster angle, and print orientation (XY, YZ, ZX). Testing in this phase was performed according to both the 12- and 60-second VBB test procedures. The number of samples evaluated varied throughout testing, but a minimum of four samples were tested for each variable combination.

2.1 Material

Within this study, several different thermoplastic polymers printed via FFF were evaluated. Materials were categorized and renamed based on the composition of their polymers. Examples of different polymer compositions include polyetherimide (PEI), polyethersulfone (PES), polyetherketoneketone (PEKK), polycarbonate (PC), acrylonitrile butadiene styrene blend (ABS), and Nylon 12. Several tested materials were a blend of different polymer compositions. The evaluated thermoplastic materials were named as follows:

1. PEI – PC: A Polyetherimide/Polycarbonate blend

2. PEI: An unreinforced amorphous Polyetherimide

3. PES: A Polyethersulfone

4. PEKK: A Polyetherketoneketone based thermoplastic

5. Nylon 12: A Nylon polymer thermoplastic

6. PC-ABS: A Polycarbonate/acrylonitrile butadiene styrene blend

7. PC: A Polycarbonate based thermoplastic

Testing was conducted on samples with the same thickness but different material types. Samples within this test series were composed of 6 inner layers (0.06 inches thick) without any exterior solid layers.

A direct comparison of recorded burn lengths and flame times between PEI-PC and PEI samples is displayed in Figure 7 and Figure 8, respectively.
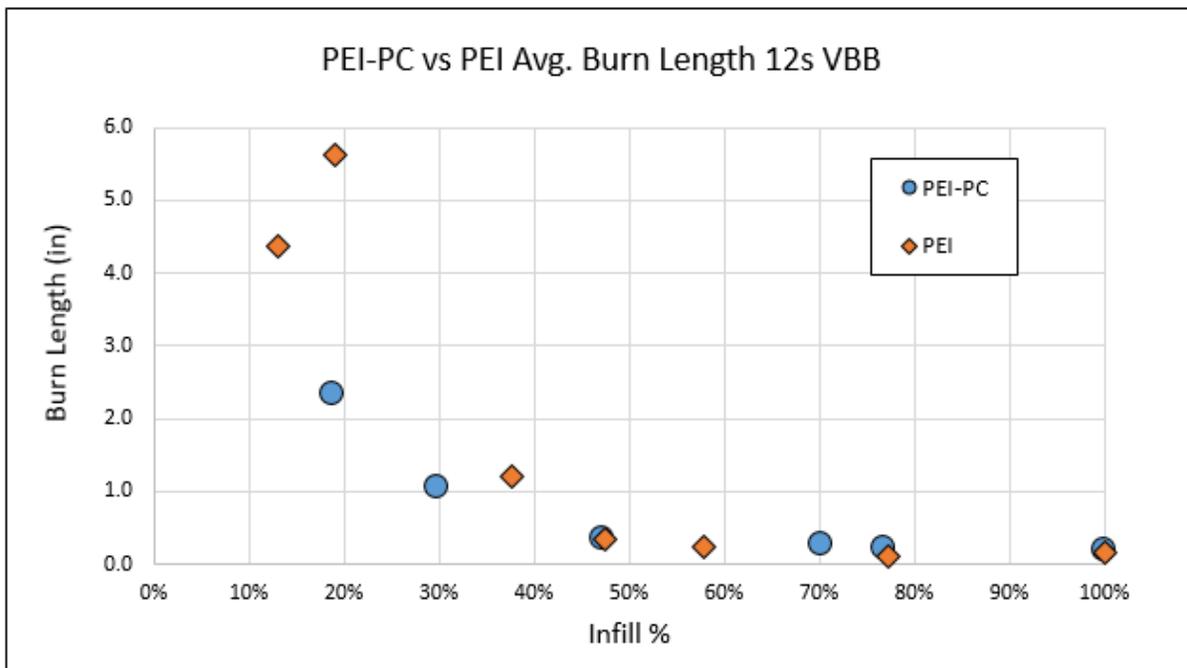
Figure 7. 12s VBB – Burn length comparisons
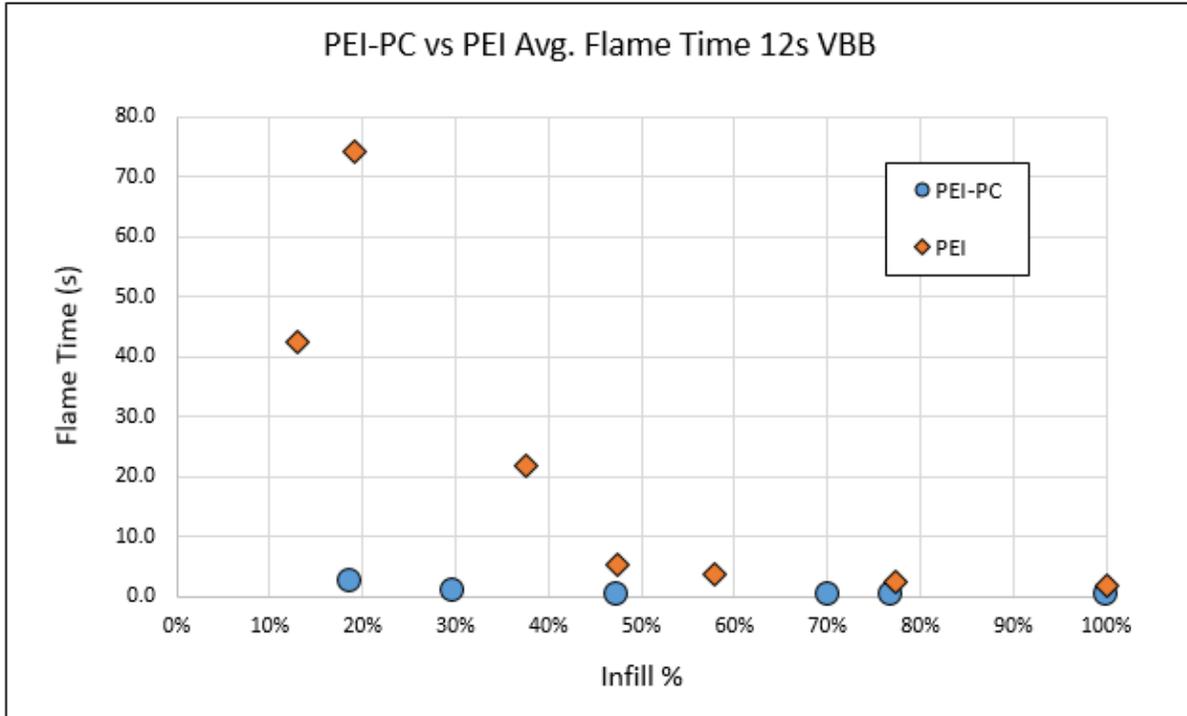
Figure 8. 12s VBB – Flame time comparisons

As expected, the material type was determined to be one of the most important parameters in predicting the flammability of the tested samples. For these tests, the two materials produced similar burn lengths at higher infill percentages (>50%). However, more substantial differences in measured burn length were observed at lower infill percentages. The PEI material recorded average burn lengths exceeding 4.0 inches at infills less than 20%. Contrarily, the PEI-PC blend material at a similar infill had an average burn length less than 3.0 inches.

Disparities between recorded flame times were also substantial. The PEI material recorded much higher flame times at low infill percentages compared to the PEI-PC blend. Significantly less disparity between the two materials' flame time was observed at higher infills.

Testing was also performed according to the 60-second VBB test procedure. A graph showing the average burn lengths and flame times for the 60-second test is shown in Figure 9 and Figure 10, respectively.
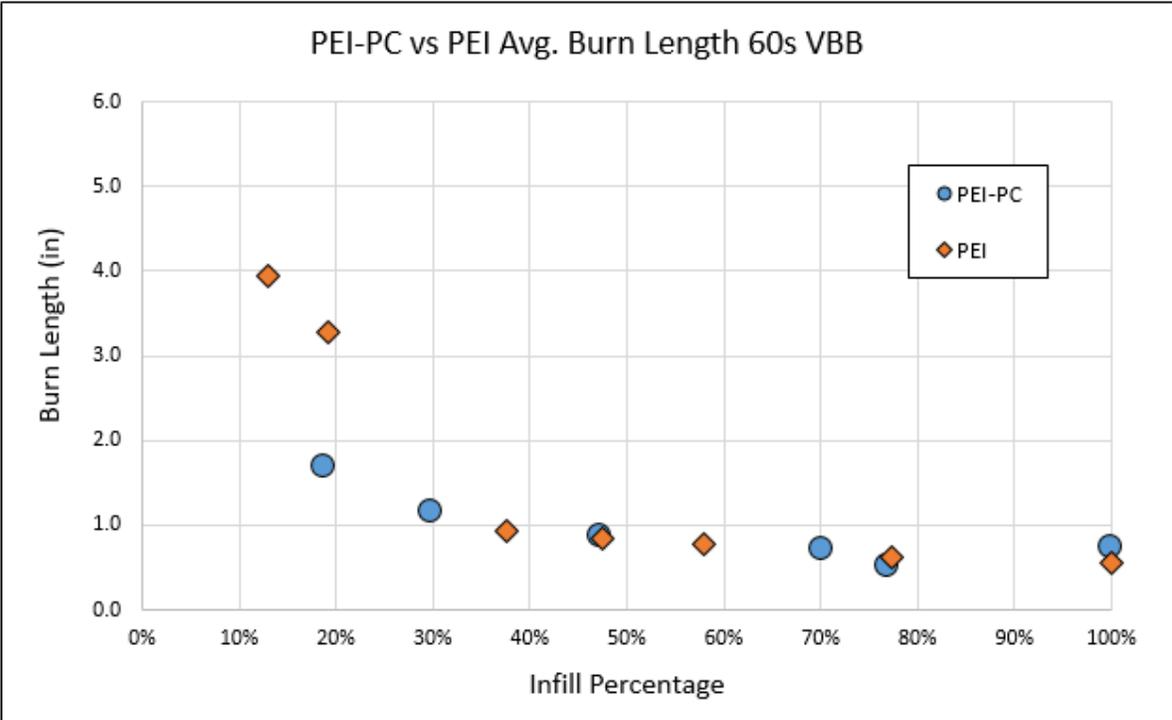
Figure 9. 60s VBB – Material burn length comparisons
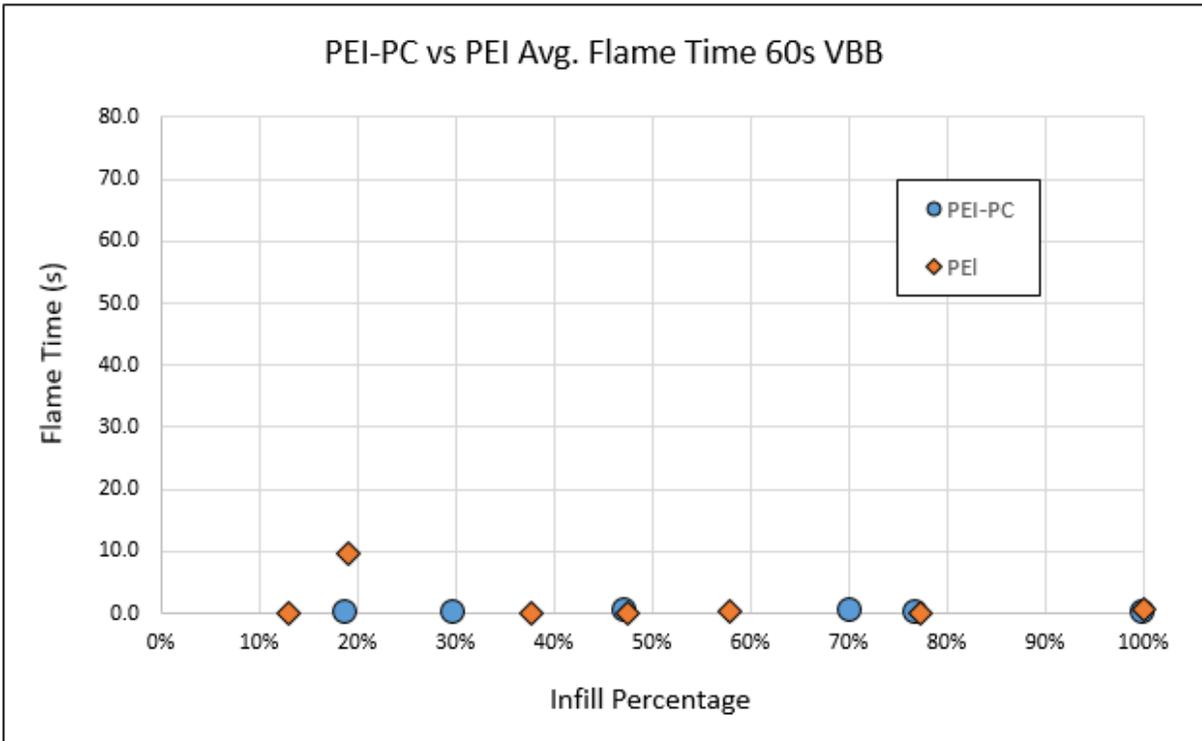
Figure 10. 60s VBB – Material flame time comparisons

9

Similar trends in measured burn lengths were observed for the 60-second tests performed. However, a significant discrepancy in recorded flame time was observed between the 12-second and 60-second VBB tests.

Throughout the 60-second VBB testing, a problem would often occur that impacted the recorded flame times. Frequently, the sample material would either melt away prior to the end of the test or drip down and block the Bunsen burner flame. Therefore, the Bunsen burner would be unable to make direct contact with the sample's remaining material and would record little to no flame time, possibly producing misleading results. Samples with less total material, such as thinner samples or those with a lower infill percentage would most often melt away. Conversely, samples with more material, such as those with a higher infill percentage or more inner layers would occasionally drip and partially block the burner flame. Images of both of these phenomena are displayed in Figure 11. This issue was observed to occur during other 60-second tests throughout this study as well.

Figure 11. Sample melted away (left) and melted material blocking Bunsen burner flame (right)

Results indicate that flame times for the 60 second tests were much lower than the 12 second tests for both materials. However, this is most likely not a realistic scenario and the reasoning for this disparity is most likely due to the problem described above.

The material type was observed to be a critical factor in determining the drip flame time. Many of the tested materials did not record a drip flame time as no flaming material fell to the bottom of the test chamber. Amongst the materials in which a drip flame time was observed, the type of material affected the way in which the sample fell to the bottom of the test chamber. Materials such as Nylon 12 were observed to drip in a liquid like manner, in which many drips of flaming material would occur sporadically. Conversely, materials such as PEI were observed to have single solid pieces of the samples fall to the bottom of the test apparatus and burn continuously.

2.2 Sample thickness (number of inner layers)

Testing was conducted to determine how variations in the thickness of a sample affected data. Throughout this study, all printed samples had a layer thickness of 0.01 inches, therefore, the number of layers directly correlated with the thickness of the sample. For example, a sample with six layers would have a thickness of 0.06 inches. The thickness of an extruded layer can be altered slightly, but that parameter was not evaluated within this study.

It was found that thicker samples recorded significantly lower burn lengths and flame times. Within these tests, two PES samples of different thicknesses (0.10 and 0.25 inches) were printed and tested. Figure 12 and Figure 13 show the data averages of the recorded burn lengths and flame times, respectively, at various infill percentages.
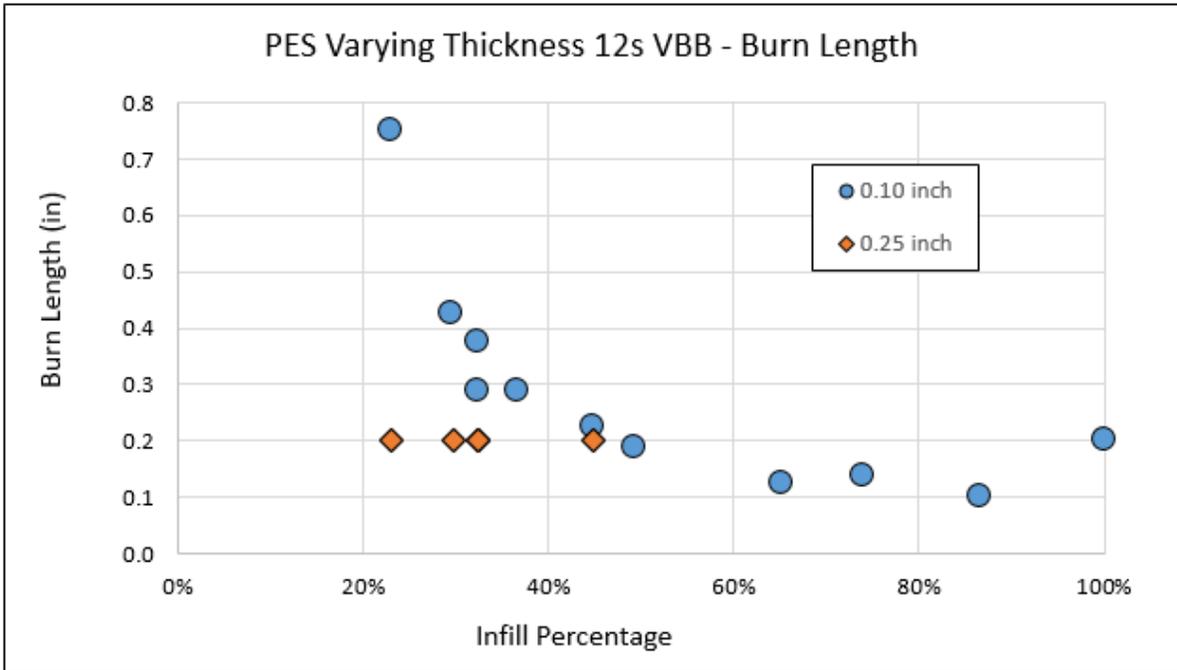
Figure 12. PES inner layer comparison – burn length
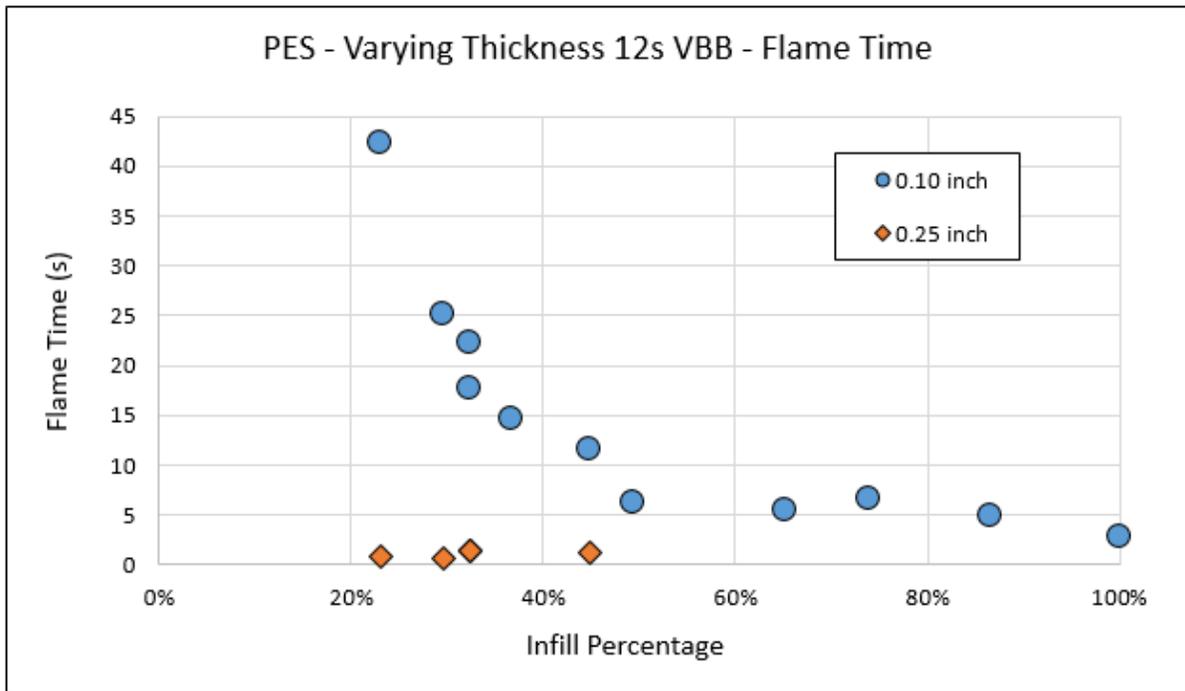
Figure 13. PES inner layer comparison – Flame time

Samples of 0.25-inches were observed to record much lower burn lengths and flame times at low infill percentages. This was particularly noticeable for the recorded flame times. At 20% infill, 0.10-inch samples recorded average flame times exceeding 40 seconds. Conversely, the 0.25-inch samples recorded flame times of less than 5 seconds with the same infill percentage.

Typically, a negative correlation between the infill percentage and burn length and flame time was observed to occur as infill percentage increases. However, no significant differences between the burn lengths and flame times of the 0.25-inch samples were observed as infill was varied between 20% and 45% infill samples. Further testing of 0.25-inch samples with greater than 45% infill was not conducted as burn length and flame time were already near minimum values.

Lastly, a significant difference in recorded drip flame times were observed between the two sample thicknesses. At low infill percentages, the 0.10-inch samples recorded average drip flame times ranging from to 1-2 seconds. However, 0.10-inch samples with higher infill percentages did not record any drip flame time. All 0.25-inch samples did not record drip flame times, including the samples with lower infill percentages. This suggests that the thickness of a sample and the infill percentage are important factors in predicting if a sample will record a drip flame time.

2.3 Infill percentage

Infill percentage is the percent of the interior of a 3D printed part that is composed of material. Testing was conducted on 0.06-inch thick PEI-PC blend samples that were composed entirely of "infill" and were not printed with solid outer layers. During the production process, the spacing between the rasters was altered to produce samples with various infill percentages. VBB testing of 12 and 60 seconds was performed for these samples. The average recorded burn length and flame times of these samples for the 12 second test series is displayed in Figure 14.
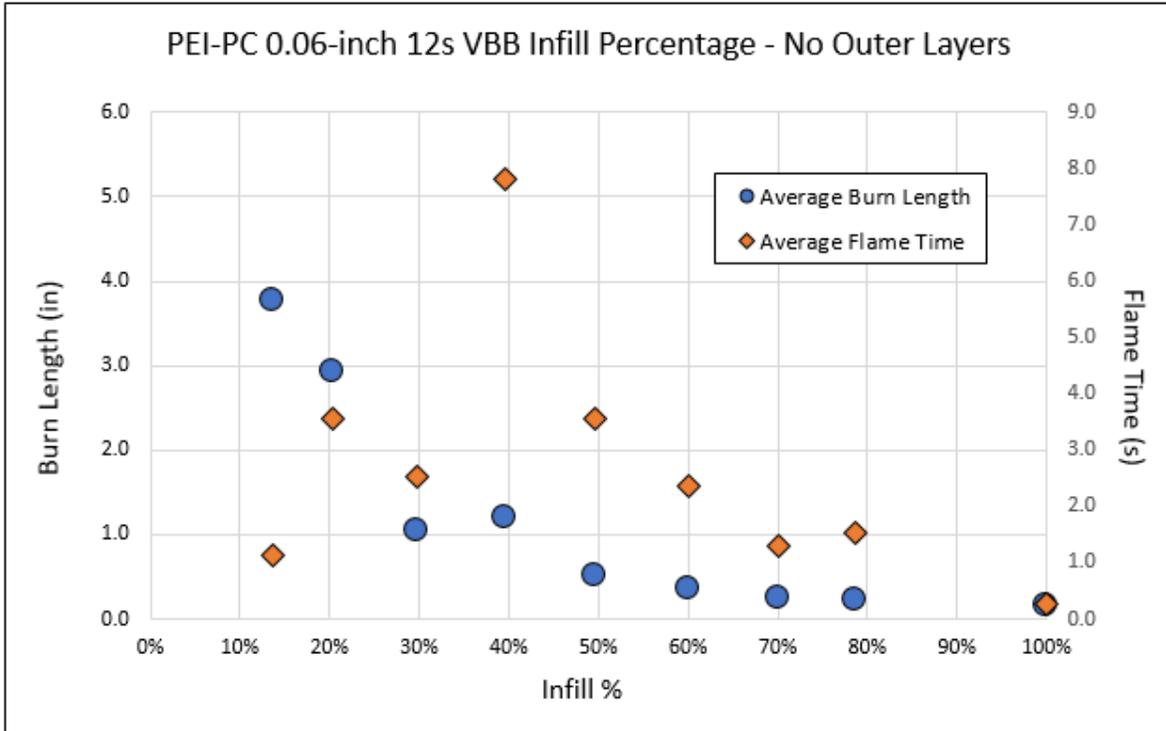
Figure 14. Infill comparisons - PEI-PC – 12s VBB tests

A clear trend in burn length was observed as infill percent was varied. Generally, as infill percent increased, the measured burn length decreased. This inverse correlation between infill percentage and burn length was observed throughout other tests as well.

Figure 14 above indicates that recorded flame times peaked at 40% infill and samples within the 10-30% range experienced low flame times. However, samples within the 10-30% infill range may have produced misleading flame time results. Frequently, the material of the samples within this infill range would melt away prior to the end of the test. Therefore, the Bunsen burner flame was unable to make direct contact with any of the remaining material and would record a low average flame time.

The recorded burn length and flame time of the 60 second test series is shown below in Figure 15.
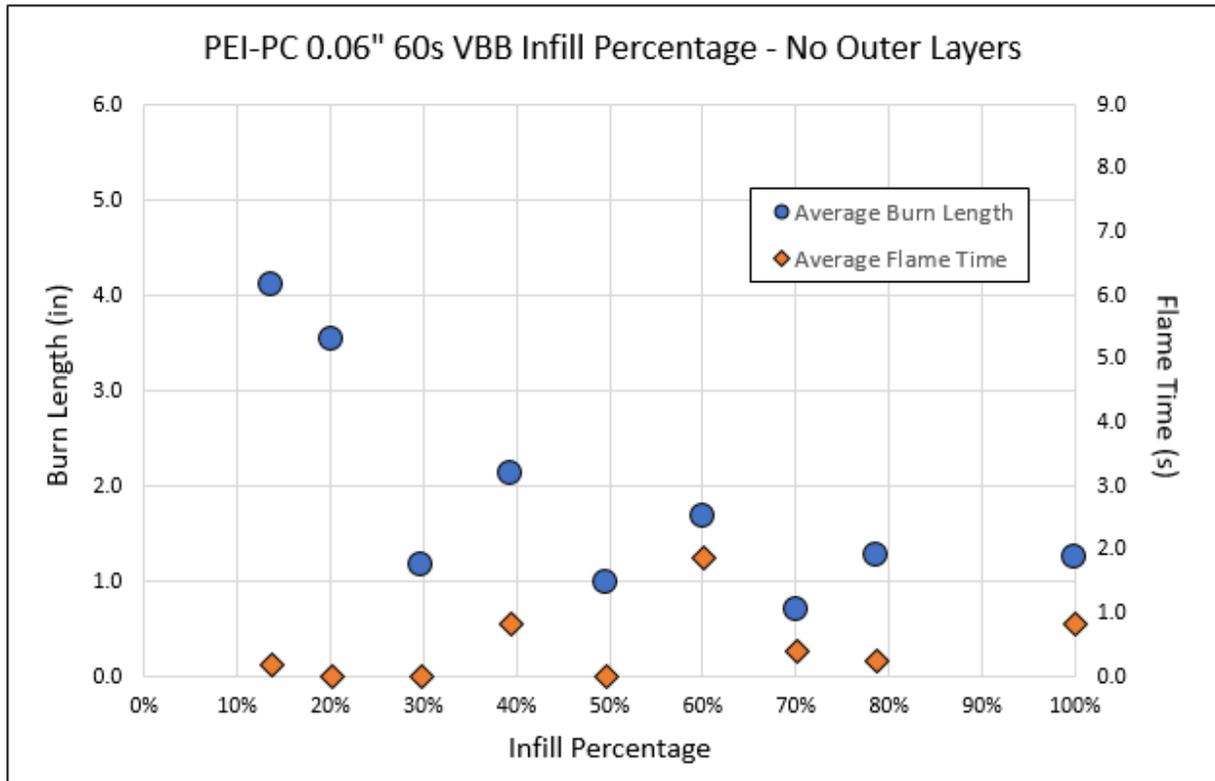
Figure 15. Infill comparisons – PEI-PC – 60s VBB tests

Similar trends in burn length were observed in the 60-second VBB testing. The average burn length gradually decreased as infill percentage increased. Samples with low infill ($< 20\%$) recorded average burn lengths exceeding 3.5 inches, whereas burn lengths for higher infills were observed to range between $0.5 - 2.0$ inches. The measured flame time of the 60s VBB samples were inconsistent and a specific trend was not clear. Tests within this series experienced a similar problem to the 12 second tests, in that samples with lower infills would melt away prior to the conclusion of the experiment.

Note: Two different individuals performed testing for the 60 second tests. Disparities between burn length data for the 30%, 50%, and 70% samples compared to the rest of the data were most likely due to this.

There was no recorded drip flame time for any of the samples of this material, regardless of the infill percentage.

Additional testing was conducted with the PEI material and similar results were observed. Figure 16 and Figure 17 show the average burn length and flame time data for the 12 and 60 second tests, respectively.
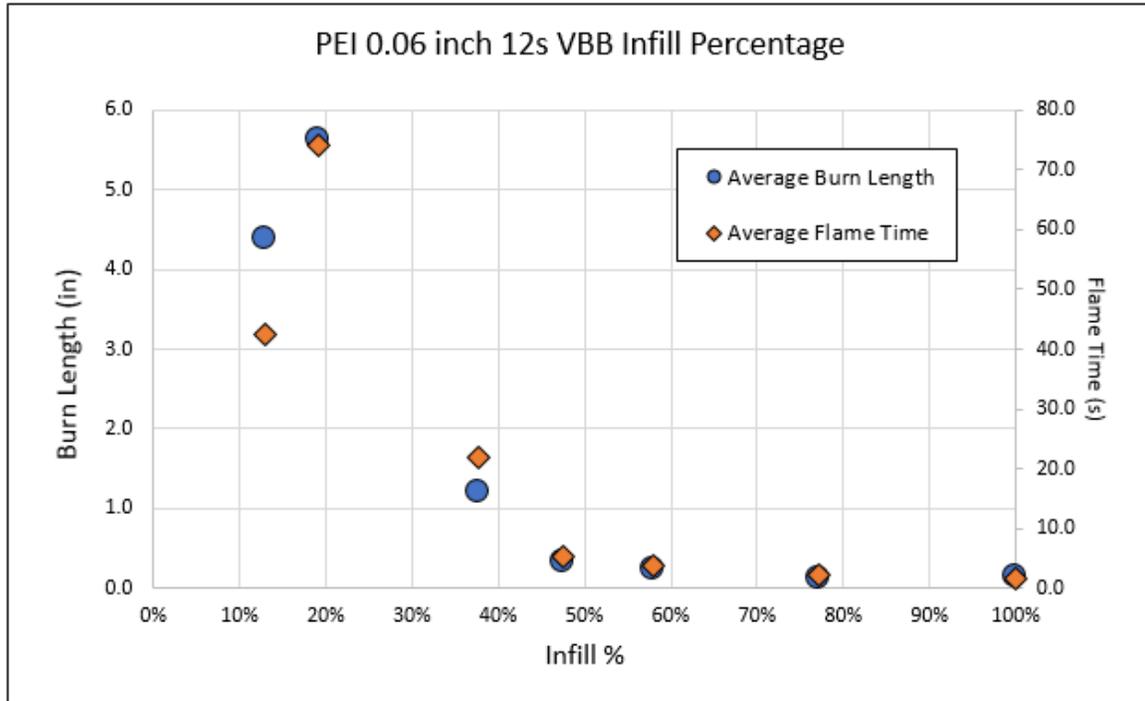
Figure 16. Infill comparisons – PEI – 12s VBB
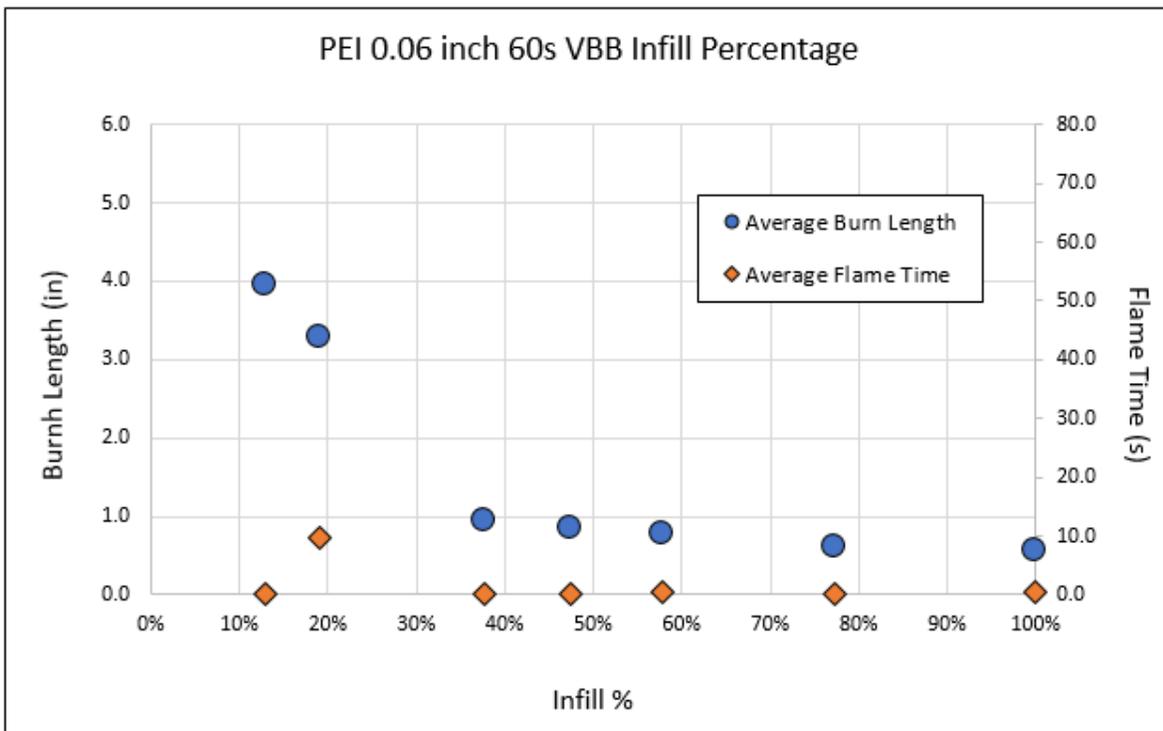
Figure 17. Infill comparisons – PEI – 60s VBB

PEI burn length and flame time trends were comparable to the PEI-PC testing – flame time and burn length decreased as the infill percentage increased. However, recorded drip flame time values differed compared to the PEI-PC test series. For the PEI tests, samples with infill percentages lower than 20% had material fall to the bottom of the test chamber and flame for an average of three seconds. Figure 18 shows the drip flame time data for the 12 second tests.

The data indicates that samples produced at lower infills may be more likely to record drip flame times compared to higher infill samples. However, the material of the sample itself is still the main contributing factor.
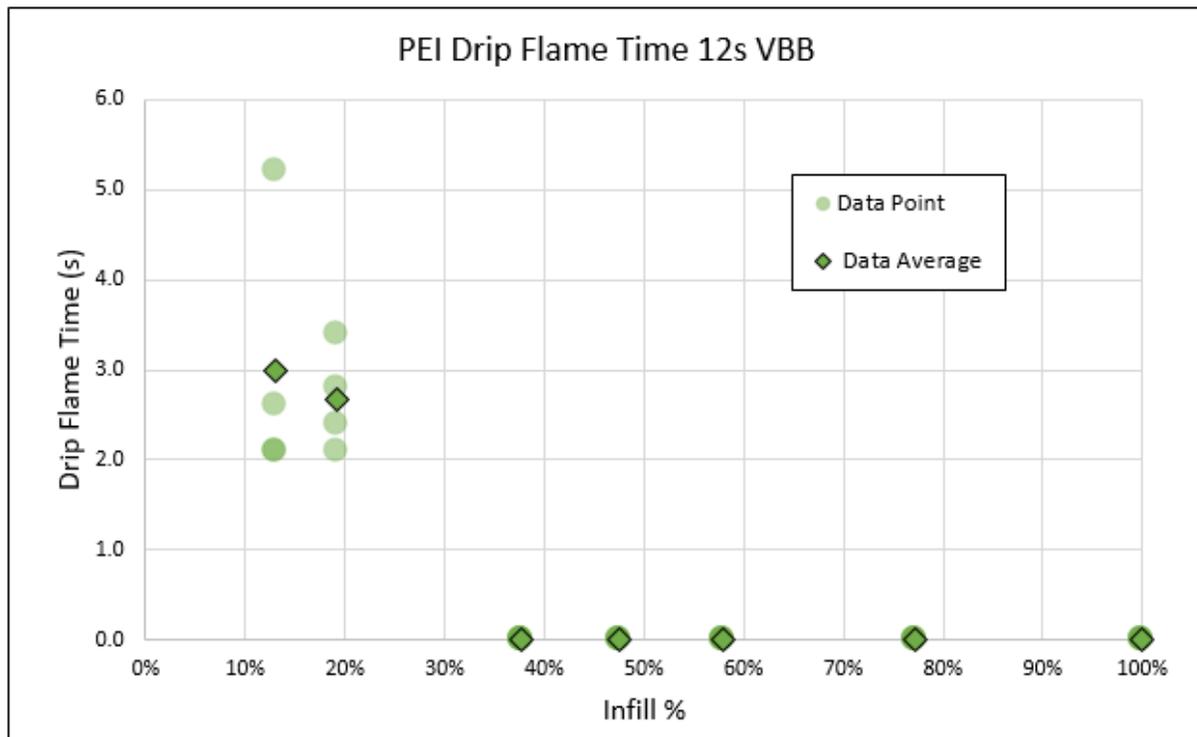
Figure 18. PEI drip flame time 12s VBB tests

2.4   Infill pattern

Samples of the PEI-PC material with a thickness of 0.10 inches were evaluated according to both the 12-second and 60-second VBB test procedures. Each sample was composed of six inner layers with various infill patterns and two solid outer layers on each side. All infill patterns had an infill percentage ranging from 20 to 35%, with the exception of the solid samples, which had a 100% infill percentage. The average recorded burn length and flame time for the samples in both the 12- and 60-second tests are shown in Figure 19 and Figure 20, respectively. There was no drip flame for any of the recorded samples.
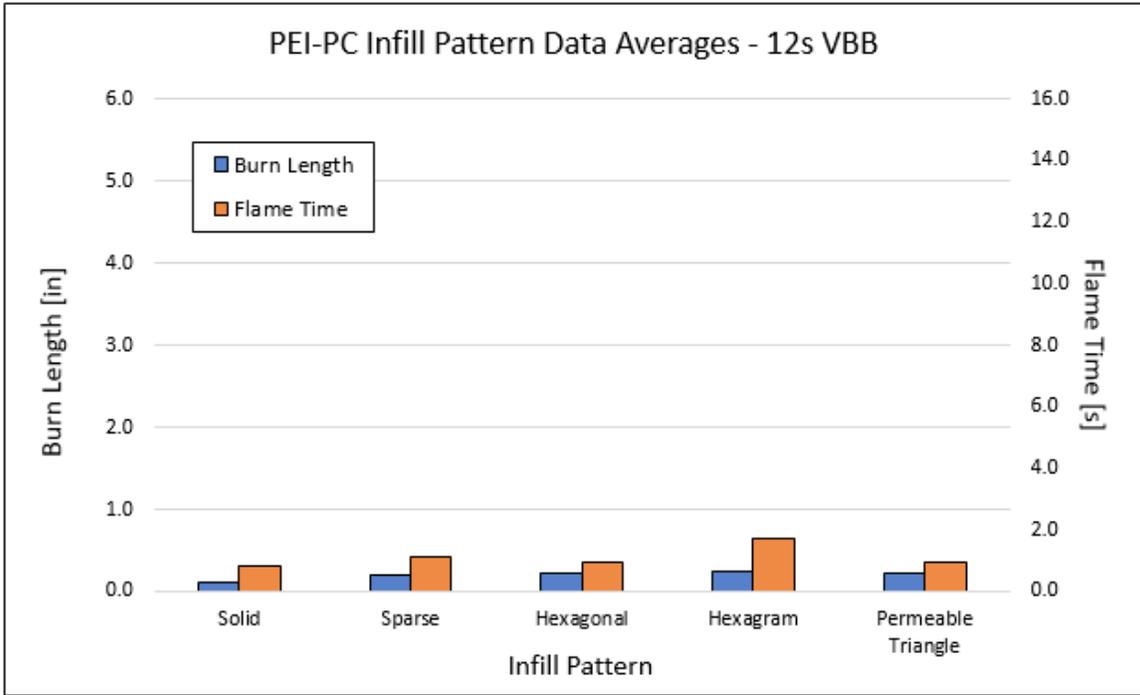
Figure 19. 0.10-inch PEI – PC infill comparisons - 12s test data
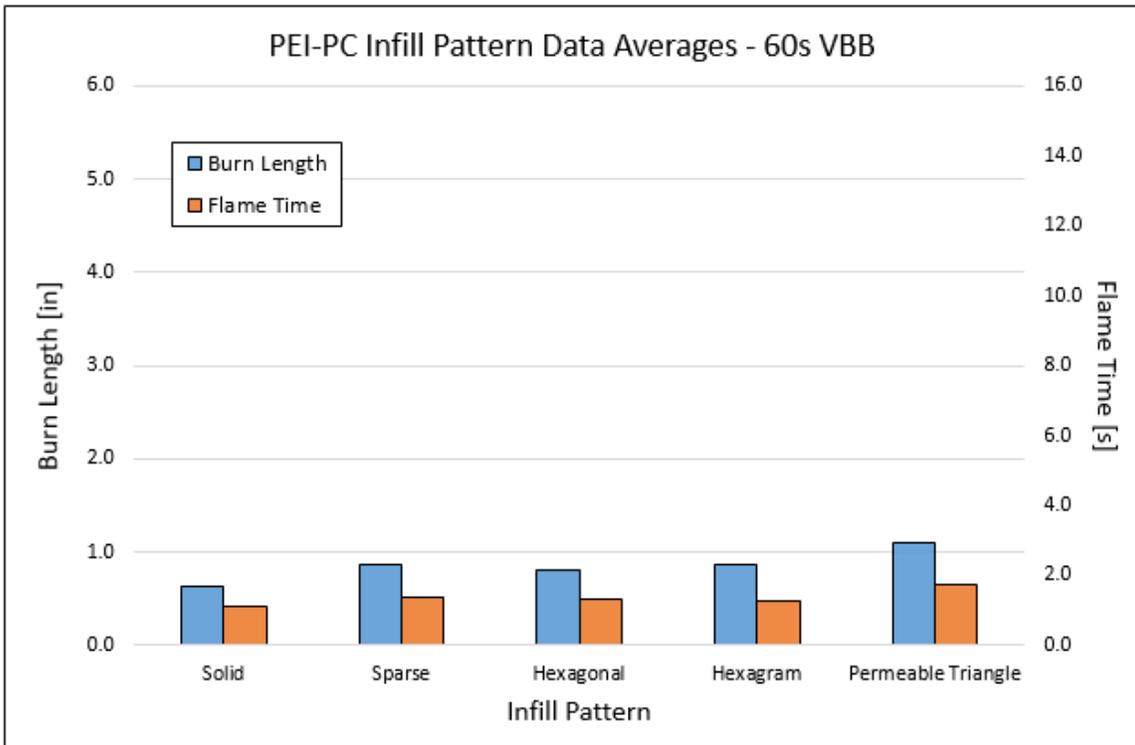
Figure 20. 0.10-inch PEI – PC infill comparisons - 60s test data

Within the 12-second test data, minimal differences in average recorded burn lengths were observed when infill patterns were varied. Average burn lengths varied from 0.10 inches to 0.25 inches depending on the infill pattern. The solid samples recorded the lowest average burn length and hexagram recorded the highest. Similar results were observed for flame time data.

Similar to the 12-second tests, very little change in results was observed as infill patterns were altered throughout the 60-second tests. The solid infill pattern was once again found to have the lowest recorded burn lengths and flame times, while the permeable triangle infill pattern recorded the highest burn length and flame time within this test series. Overall, only minimal differences between recorded data were observed as infill patterns were altered for the PEI-PC material.

2.5 Raster width

In the next phase of testing, samples of the PEI-PC blend with a thickness of 0.06 inches were tested. All samples were printed with a raster angle of 45°/45° and composed of either solid or sparse infill patterns at varying infill percentages. Raster widths were then altered to three different levels (0.016, 0.022, and 0.030 inches) and evaluated. A minimum sample size of four for each raster width/infill percent combination was tested. Recorded burn length and flame time of the resulting data is shown in Figure 21 and Figure 22 for the 12-second tests.
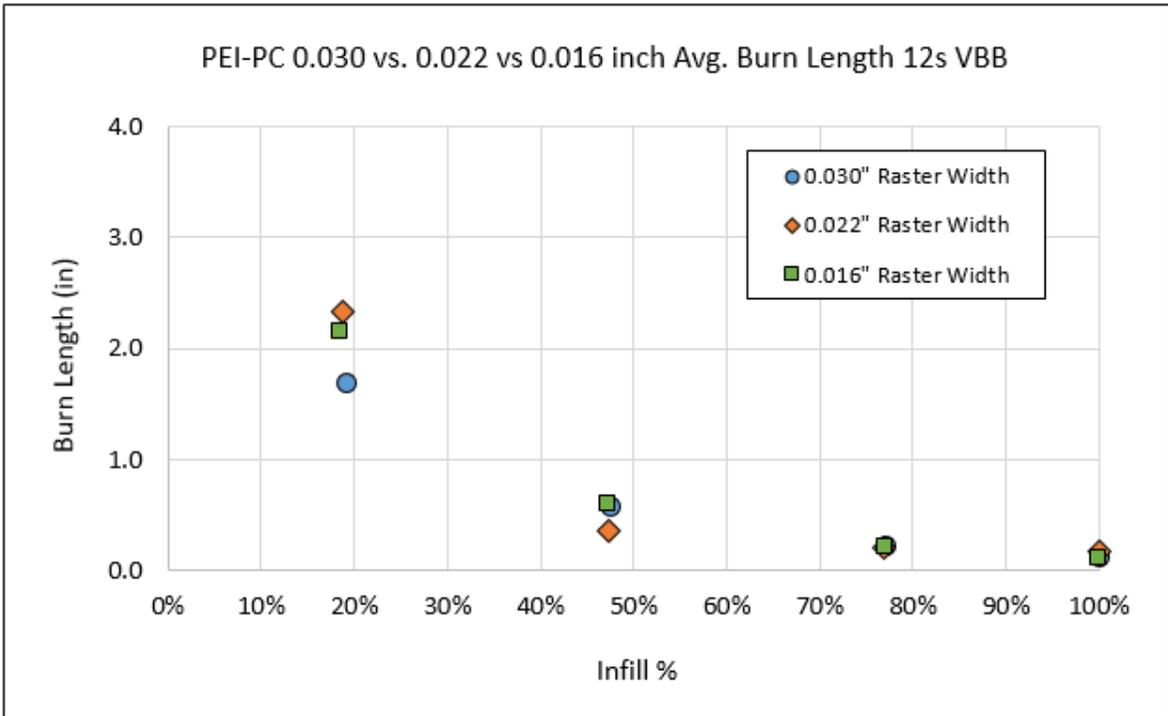
Figure 21. Raster width burn length – 12s VBB tests
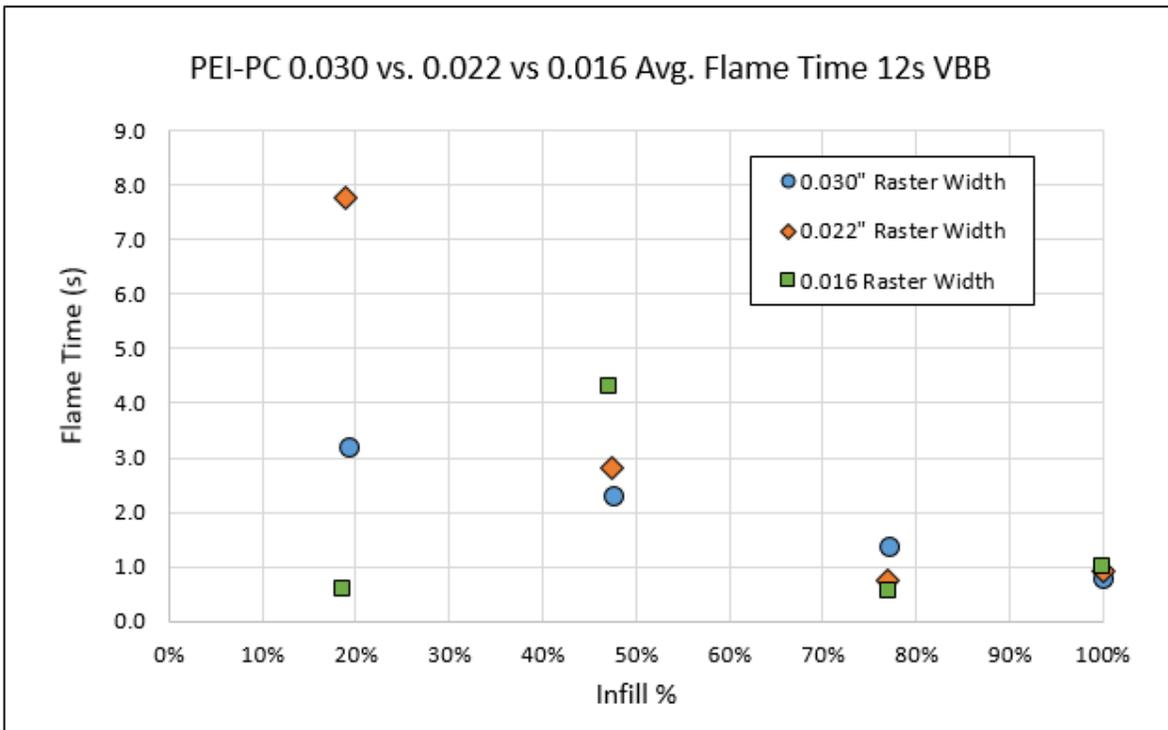
Figure 22. Raster width flame time – 12s VBB tests

Similar to previous tests, the infill percentage was found to be the biggest determinant in predicting flammability. However, it was evident that variability between raster widths was most prevalent at lower infill percentages. Although variations in raster width were observed to cause disparities in recorded data at low infills, no direct trend from alterations in raster width was observed to affect test results directly.

For example, the 0.016-inch raster width samples were observed to have the lowest flame time at 20% infill. However, at approximately 50% infill the 0.016-inch samples were found to have the highest flame time of all three raster width levels. More variability was observed in recorded flame times compared to burn lengths.

Additional testing was performed on samples according to the 60-second VBB test method. Similar trends to the 12-second tests were observed for the recorded burn lengths. However, there was no clear trend in recorded flame time, as the average flame time for all samples did not exceed 0.50 seconds, despite changes in the raster width/infill percent combinations.

The only samples that recorded any drip flame time within this phase of testing were the 0.016-inch samples at the lowest tested infill % (18.6%). A graph showing the recorded drip flame times of the 0.016-inch samples for the 12 and 60 second VBB tests is shown in Figure 23 and Figure 24.
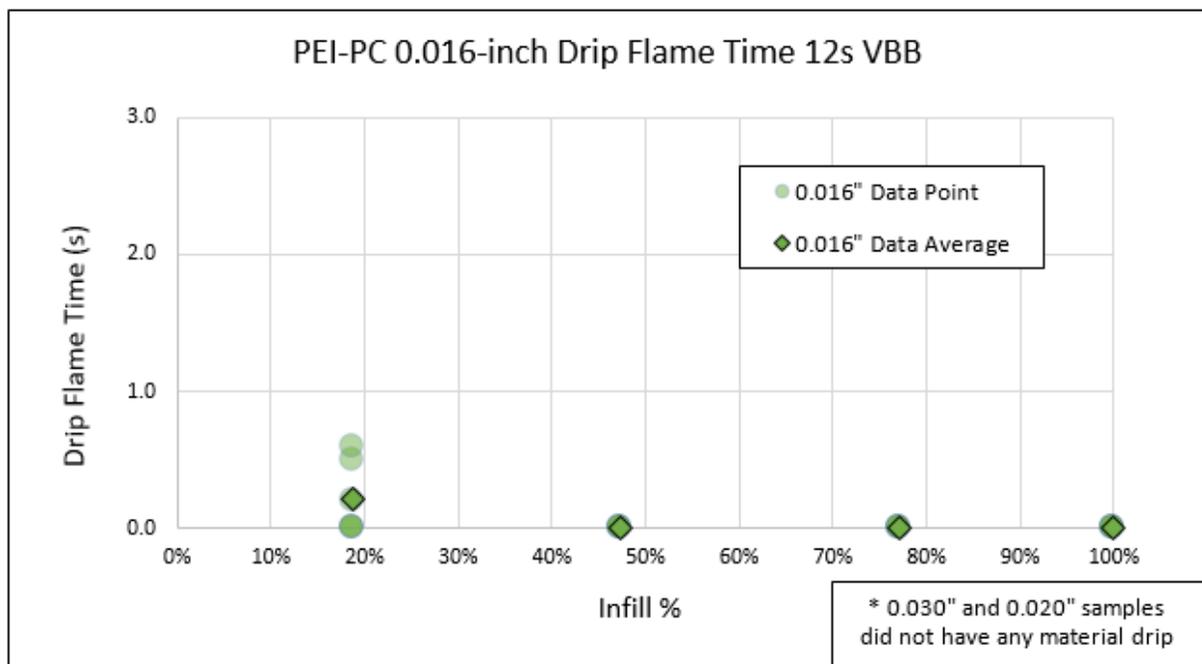
Figure 23. Raster width drip flame time – 12s VBB tests
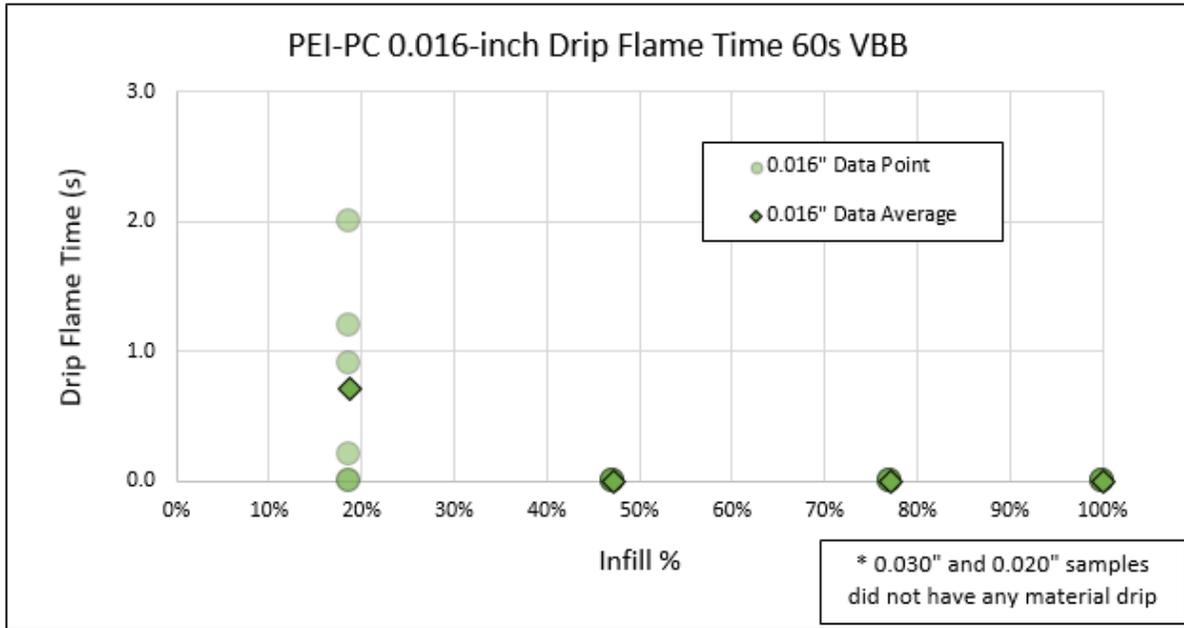
Figure 24. Raster width drip flame time – 60s VBB tests

For this combination, the average drip flame-time was 0.22 seconds and 0.72 seconds for the 12- and 60-second VBB test, respectively. This suggests that thinner raster widths at lower infills may be more susceptible to dripping.

2.6   Raster angle

In order to evaluate raster angles, an experimental setup similar to the raster width testing was performed. Three different raster angles were evaluated (90°/0°, 60°/30°, and 45°/45°) at various infill percentages. A minimum sample size of four samples for each combination was tested. The raster width of all samples was kept constant at 0.022 inches. Furthermore, the tested material, PEI-PC, was used throughout all tests. Figure 25 and Figure 26 show the average burn length and flame time results for the 12-second tests, respectively. Figure 27 and Figure 28 displays the average data results for the 60-second tests.
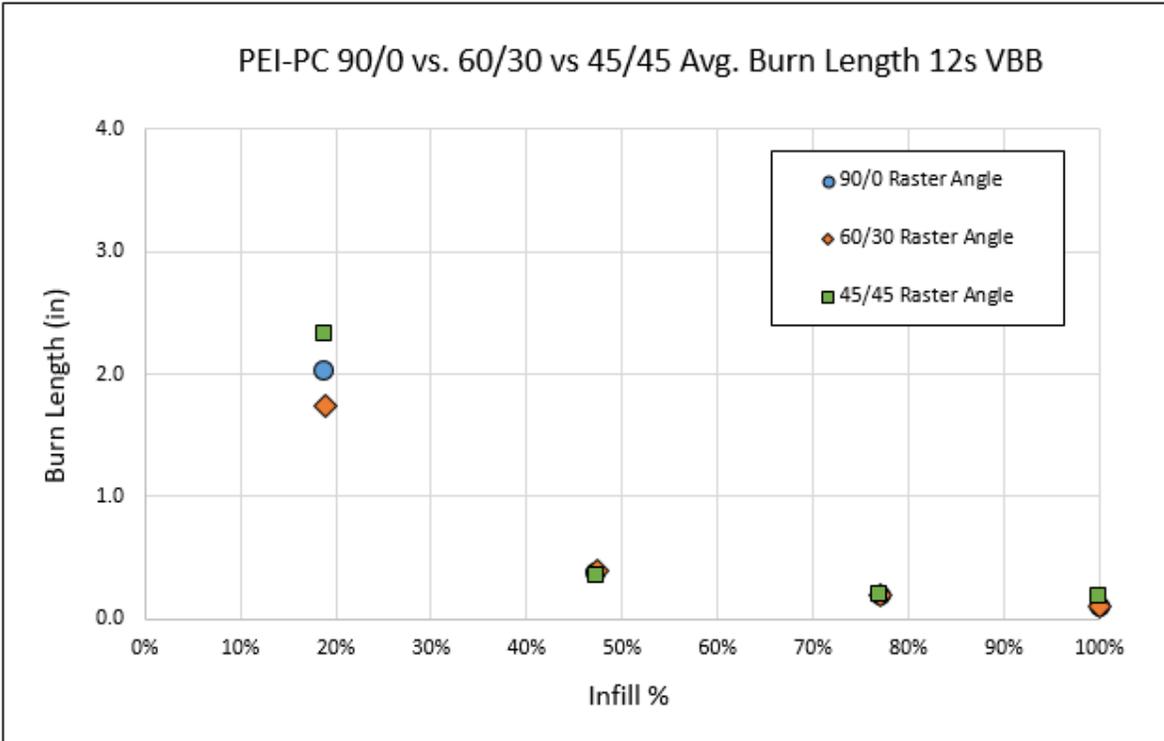
Figure 25. Raster angle burn length – 12s VBB tests
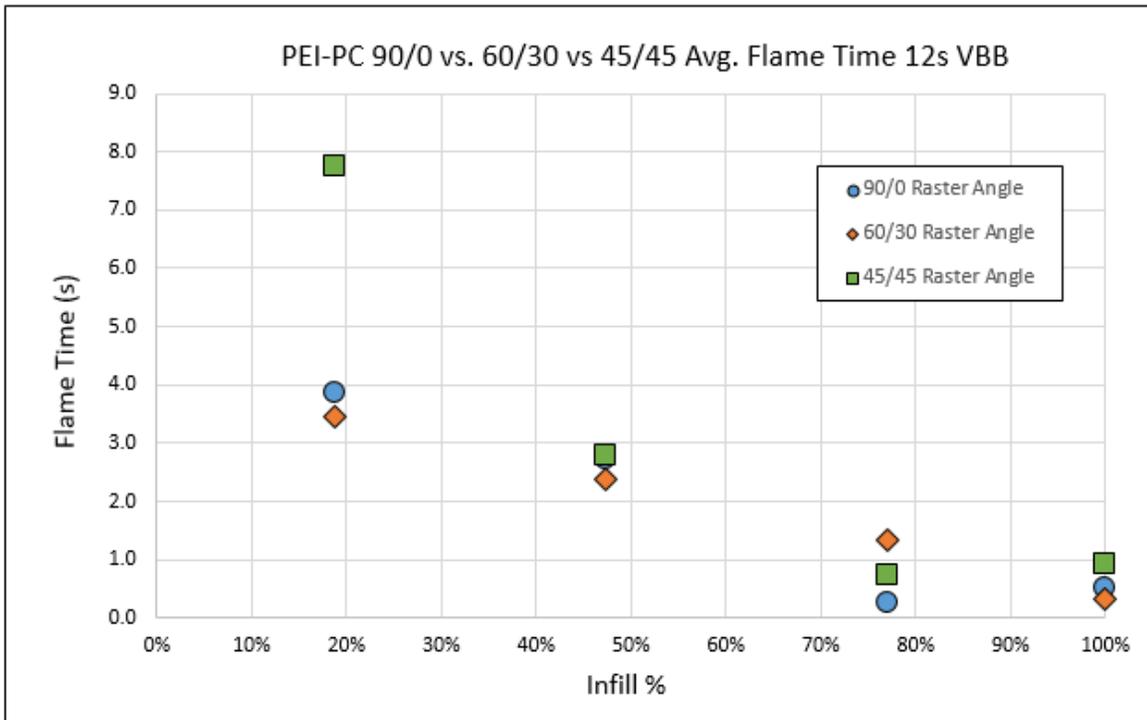
Figure 26. Raster angle flame time – 12s VBB tests
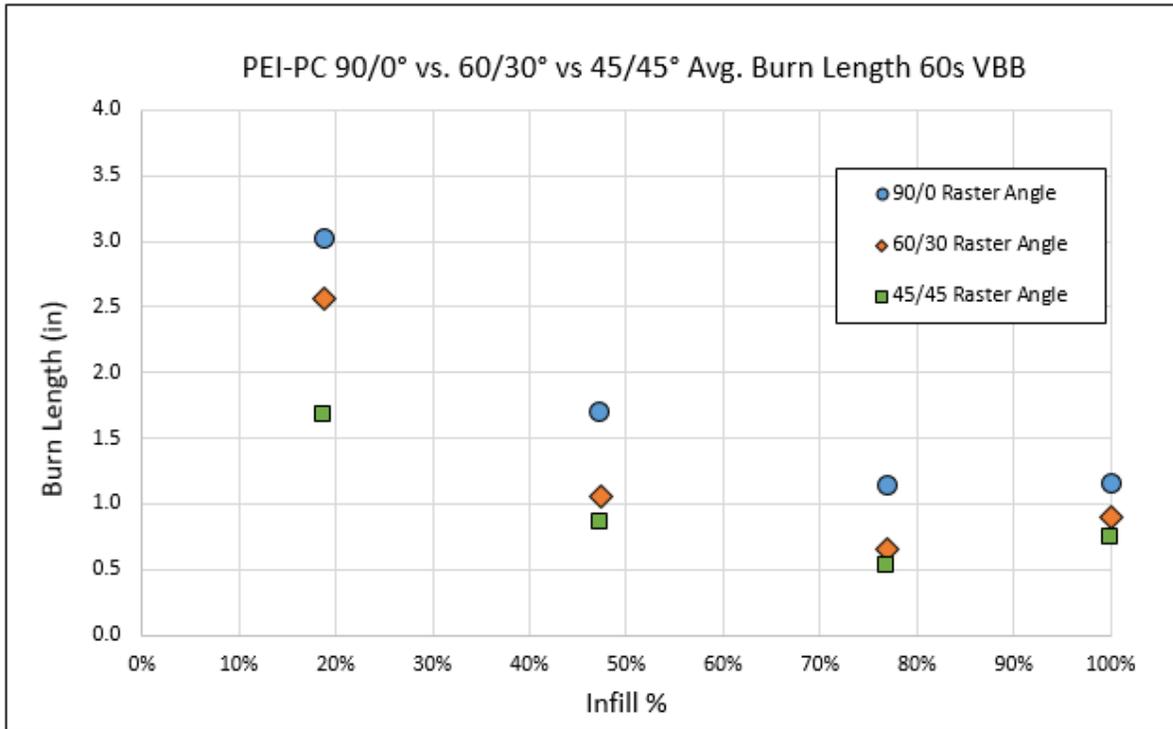
Figure 27. Raster angle burn length – 60s VBB tests
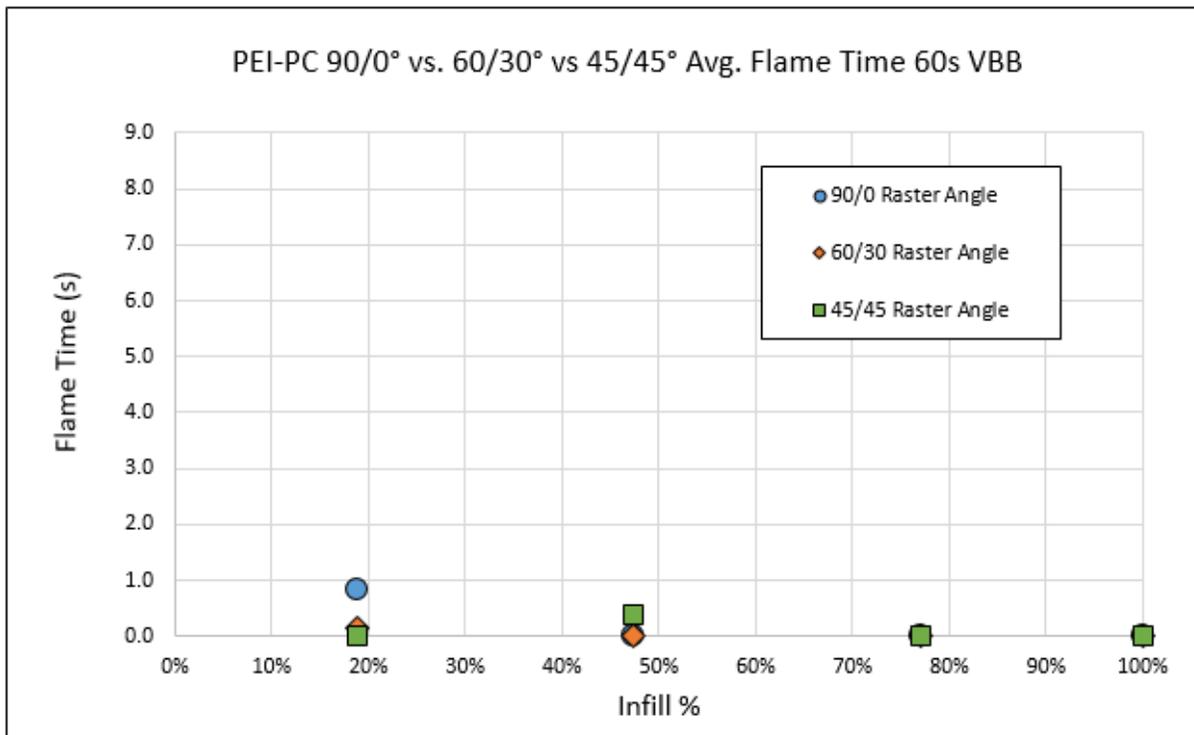
Figure 28. Raster angle flame time – 60s VBB tests

Testing from the 12-second experimentation produced similar results to the raster width results. High amounts of variability between raster angles was observed at lower infill percentages for both burn length and flame time. There were no clear trends displayed between raster angle and the recorded flame time. On the contrary, burn length data produced from the 60-second test did provide a clear trend in data. For these tests, the 90°/0° raster angle consistently produced a higher burn length for all tested infill percentages and the 45°/45° angle samples had the lowest recorded burn lengths. However, this trend was only evident for burn length data, no discernable trend was observed for flame time.

Within this test series, none of the samples had any flaming material fall to the bottom of the test chamber. Therefore, no drip flame time was recorded.

2.7 Print orientation

Samples of 0.06-inches composed of the PEI-PC blend material were printed at different orientations (XY, YZ, and ZX). Charts comparing the burn length and flame time data for both the 12- and 60-second VBB tests are shown in Figure 29 and Figure 30, respectively. For the PEI-PC material, none of the samples had a recordable drip flame time.
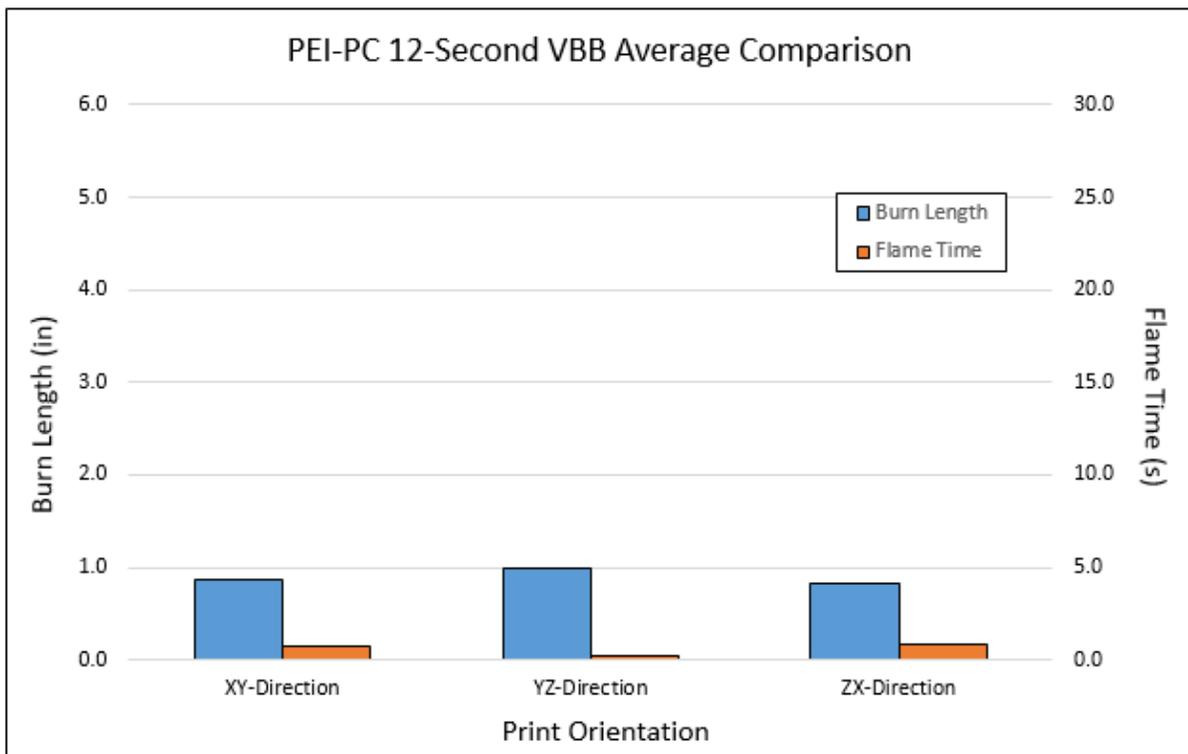
Figure 29. PEI-PC print orientation comparisons – 12s test
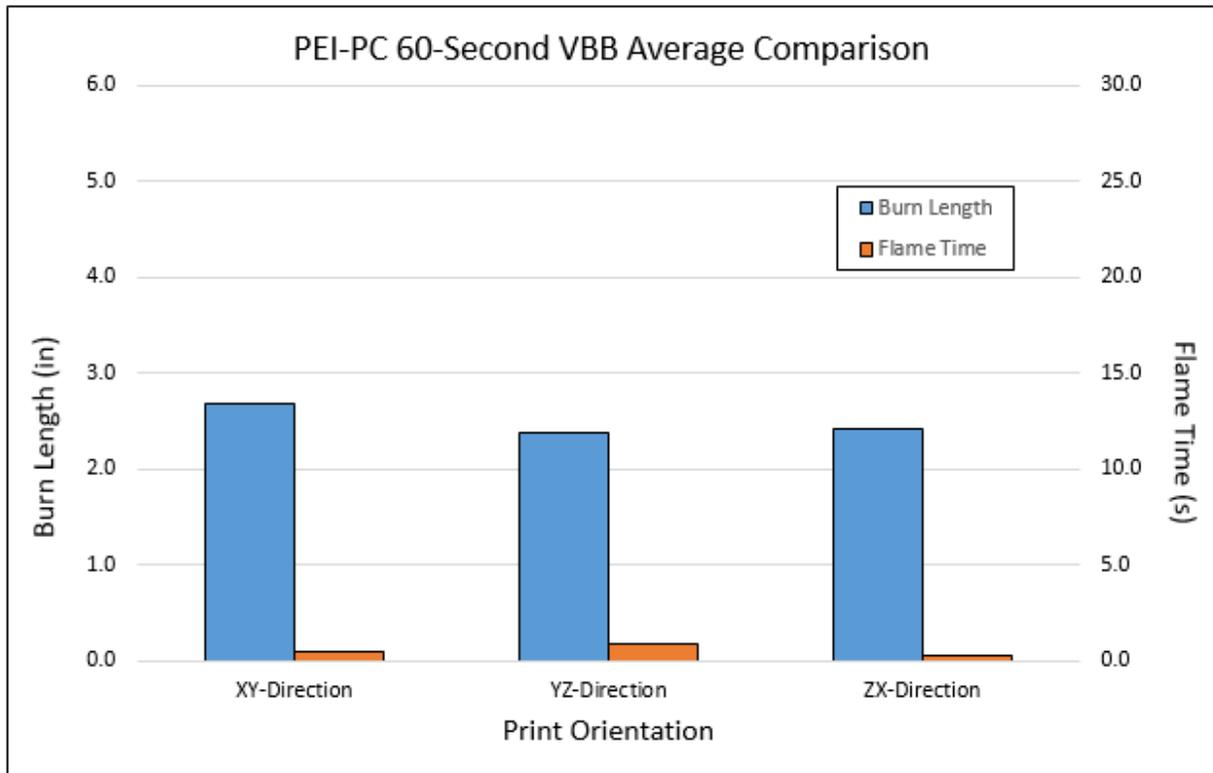
Figure 30. PEI-PC print orientation comparisons – 60s test

Results indicate alterations in the print orientation produced very little impact on the flammability of a 3D printed PEI-PC sample. For the 12-second tests, the ZX-direction samples recorded the lowest average burn length of 0.8 inches. The YZ samples had the highest average burn length of 1.0 inches. Disparities in flame time for 12-second samples were similar as well. The YZ-direction samples recorded the lowest average flame time of 0.3 seconds, whereas the XY samples recorded the highest average flame time of 0.8 seconds.

Similar relationships were observed within the 60-second test data. Disparities between recorded burn length were minor. The XY-direction samples recorded an average burn length of 2.7 inches. The YZ and ZX-direction samples both had average burn lengths of 2.4 inches. Furthermore, the YZ and ZX direction samples were determined to have only an average burn-length difference of 0.6 inches.

Print orientation comparison testing was also performed on the Nylon and PC materials. Graphs of the 12-second VBB tests for both materials are shown in Figure 31 and Figure 32.
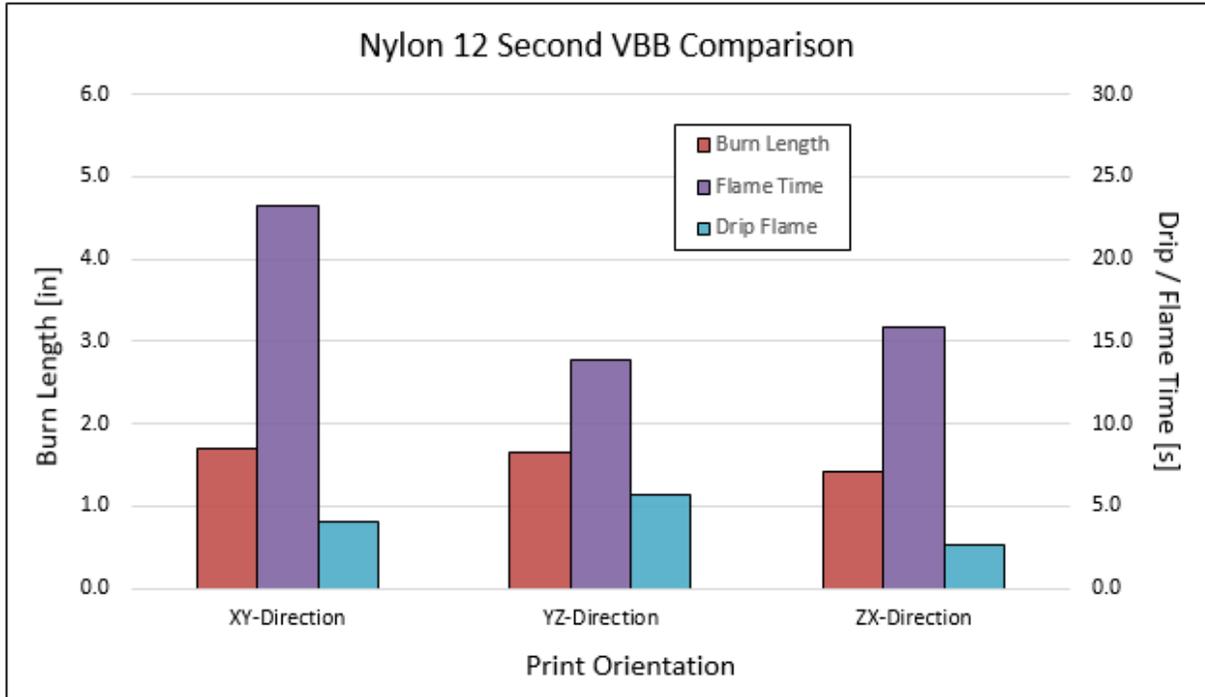
Figure 31. Nylon 12 print orientation comparisons – 12s test
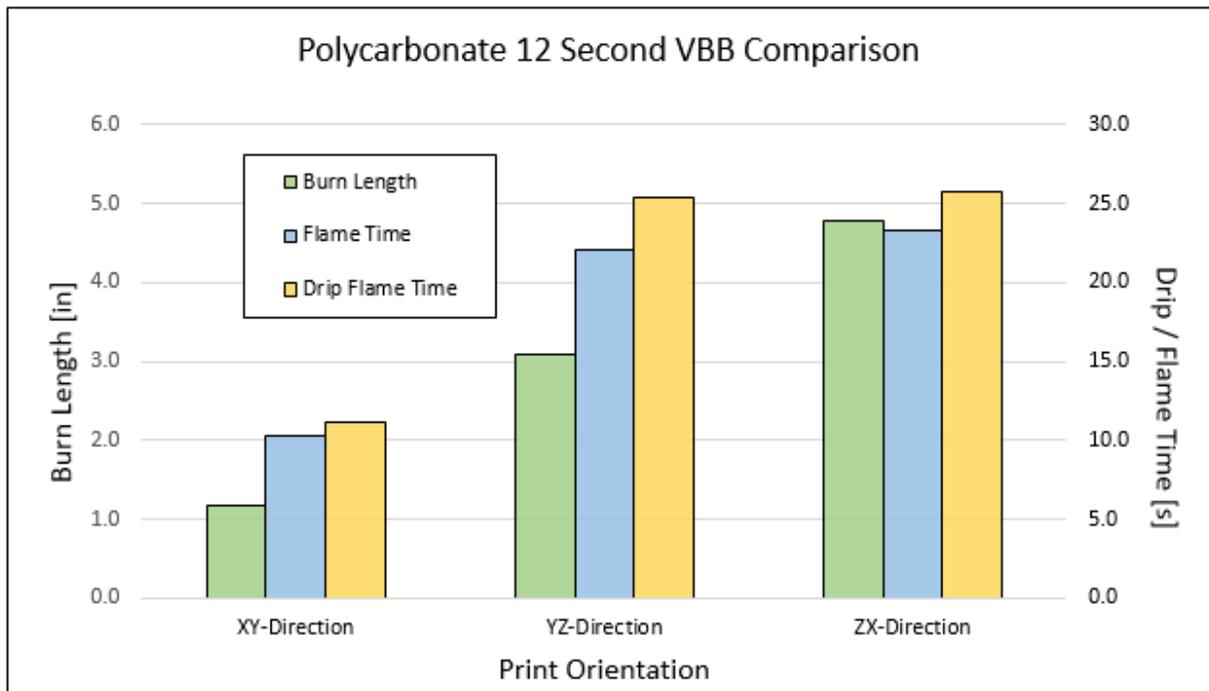
Figure 32. Polycarbonate print orientation comparisons – 12s test

Higher variance between print orientations was observed in data for these two materials. However, the observed trend in data differed depending on the material. Higher flame times and burn lengths were observed for XY-direction samples for Nylon 12. On the contrary, XY-direction samples for the PC material produced the lowest recorded data for all three metrics.

This suggests that the effect print orientation has on flammability is inconsistent and data trends may differ based upon the tested material.

3 Design of experiments (DOE)

3.1 DOE setup

A design of experiments (DOE) test setup was performed to evaluate the impact that the various print parameters had, both directly on test results, as well as the interaction effects when combined with other parameters.

Within this phase of testing, 120 16-by 3-inch samples were printed and cut into fourths, resulting in 480 4-inch by 3-inch samples being produced. Therefore, 120 unique experimental runs were produced, with 4 replicates per experiment. Within this analysis, the PEI-PC, PEI, PES, and PEKK materials were evaluated. The PEI-PC and PES samples were produced at the FAA William J. Hughes Technical Center. The PEI and PEKK materials were produced using the Stratasys Fortus 450mc printer. Figure 33 shows an image of all four material samples prior to being cut into fourths.
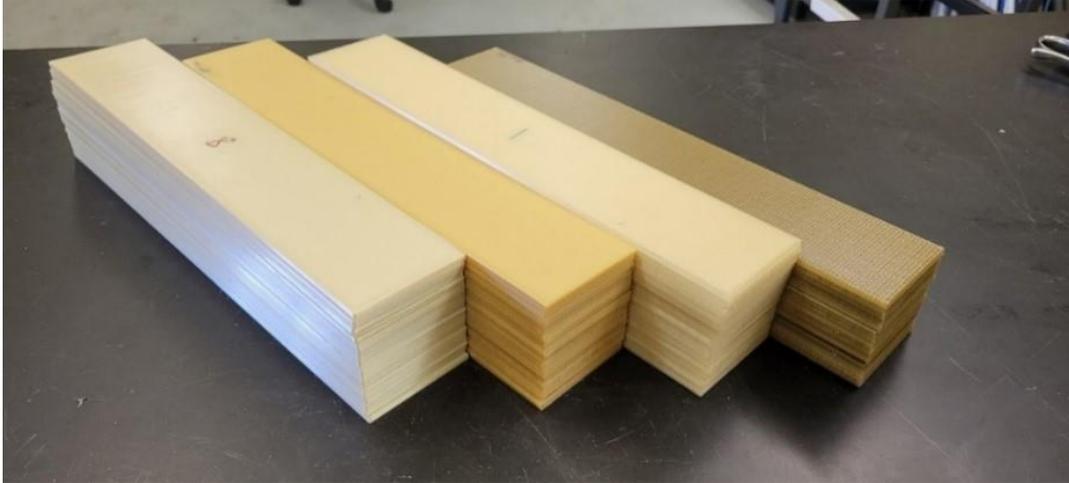
Figure 33. 16-by 3-inch precut samples – materials from left to right: PEI-PC, PEI, PES, and PEKK

All samples were tested according to the 12-second VBB test procedures. Sample test order and parameters were randomized. For these tests, the following parameters were evaluated: material type, sample thickness (number of inner layers), infill percentage, infill pattern, raster width, and raster angle. Print orientation, which was evaluated in the previous test phase, was not included. All samples were printed flat in an XY orientation.

Samples were printed at three different amounts of inner layer thickness, specifically 0 inner layers (0.02 inches thick), 4 inner layers (0.08 inches thick) and 11 inner layers (0.15 inches) thick. The 4 and 11 inner layer samples had two solid layers on each side of the sample. However, the 0 inner layer samples were composed only of two solid layers. All layers had a thickness of 0.01 inches. An image of the three different sample thicknesses is shown below in Figure 34.
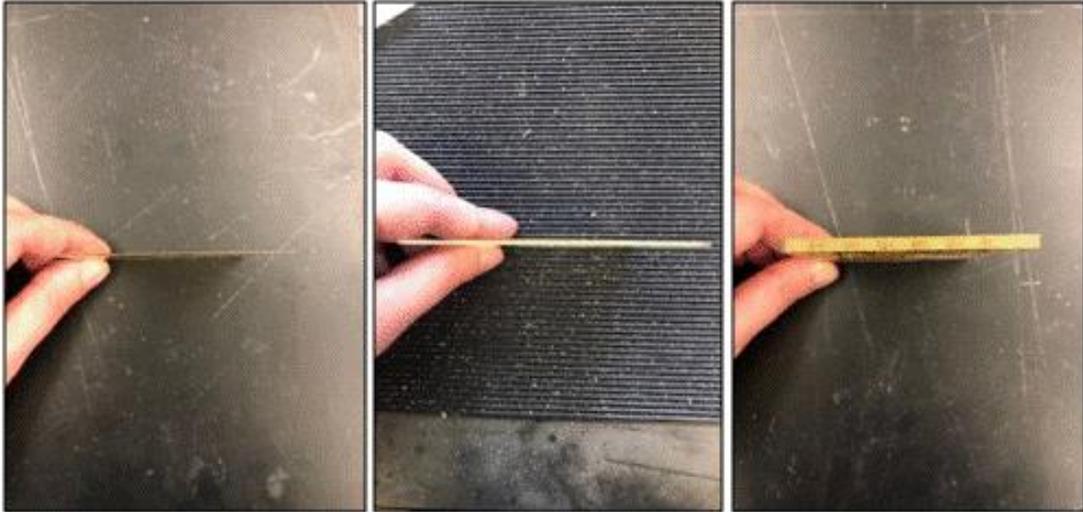
Figure 34. From left to right: 0 inner layers, 4 inner layers, and 11 inner layers sample

Since the 0 inner layer samples did not have any interior layers, the infill percentage was denoted as "0%" and the infill pattern was denoted as "None". However, alterations in the material, raster width and raster angle were still made with these samples.

Samples were produced at varying infill percentages. The evaluated infill percentages for this phase of testing were 0%, 20%, 60% and 100%. The infill percentage of each sample was calculated by dividing the volume of an interior layer of a sample by the volume of a "solid" layer. All samples of 4 and 11 inner layers had infill percentages of 20%, 60%, or 100%. The only samples that had an infill percentage of 0% were the 0 inner layer samples.

Table 1 shows the different evaluated levels for each variable.

Table 1: DOE testing variable combinations

Material	Number of Inner Layers	Infill	Infill Pattern	Raster Angle	Raster Width
		[%]		[°]	["]
PEI-PC	0	0	None	45	0.016
PEI	4	20	Sparse	67.5	0.018
PES	11	60	Sparse Double Dense (DD)	90	0.022
PEKK		100	Hexagram		0.030

Originally, only three levels for raster width (0.016, 0.022, and 0.030 inches) were going to be evaluated for this test series. However, due to constraints with the 3D printer, the raster width for the PEKK material could not be lowered to less than 0.018 inches. Therefore, all 0.016-inch samples of the PEKK material were changed to 0.018 inches.

Furthermore, an additional change was implemented. During the sample build process, it was noted that the cell size of hexagram patterns for 0.016- and 0.018-inch samples could not be decreased enough to produce a sample with 60% infill. Therefore, these samples were not produced. This omission did not include 60% infill samples with a 0.030-inch raster width.

3.2 DOE results

A statistical analysis of the collected DOE data was performed by Boeing (Mokalled & Basu, 2022). Analysis determined that an interaction effect exists for many of the evaluated parameters. This means the effect of a parameter on both the flame time and burn length depends on the level of another parameter. A confidence level of 90% was used to determine significance in this model. The full analysis can be found within Appendix A.

Graphs displaying the two-way interaction effects of the covariates versus the burn length and flame time data were created. Figure 35 shows the two-way interaction effects between material/infill percentage and material/sample thickness versus the burn length, respectively. Figure 36 shows the two-way interactions effects between material/infill percentage and material sample/thickness versus the flame time, respectively. Graphs displaying the interaction effects between all variable combinations can be found within the Appendix.
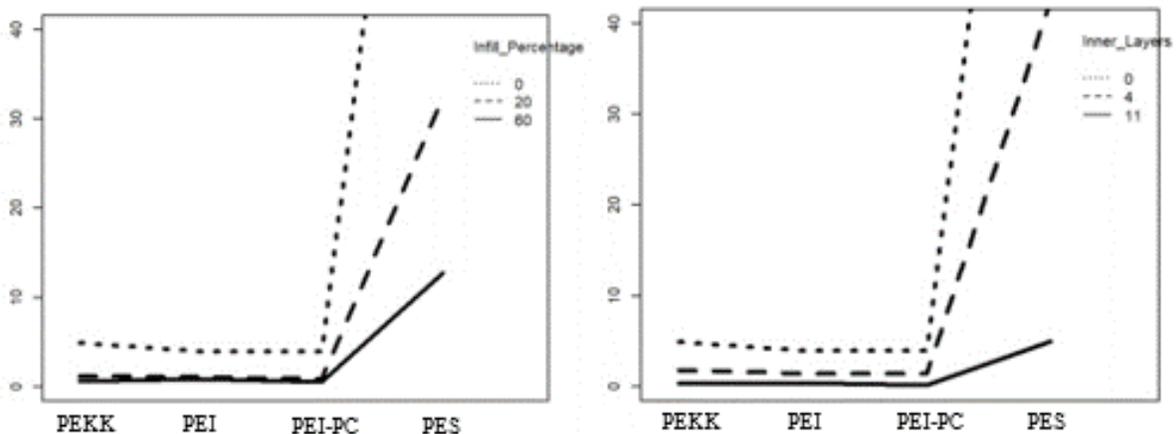
Figure 35. Material/infill percentage (left) and material/sample thickness (right) covariates vs flame time
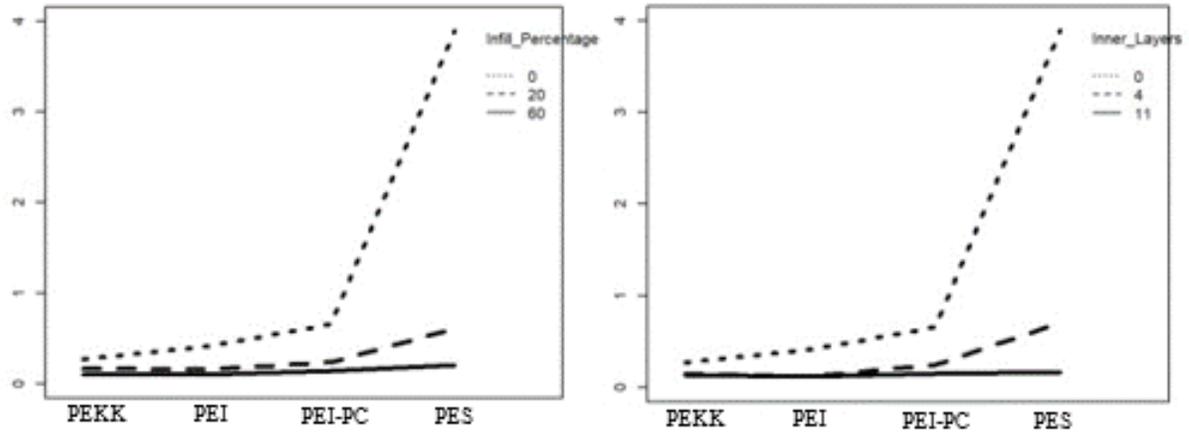
Figure 36. Material/infill percentage (left) and material/sample thickness (right) covariates vs burn length

For further analysis of the data, data was separated into two groups - zero (0 inner layers) and nonzero (4 and 11 inner layers).

3.2.1 Nonzero layer

From the DOE analysis, it was determined that all of the evaluated parameters were significant either as main effect or interaction effect parameters in predicting burn length. Five of the six parameters were significant as main effect parameters in predicting burn length: material type, raster width, sample thickness, infill percentage, and infill pattern. Raster angle was not significant as a main effect parameter, however, it was significant as an interaction effect parameter. All six of the evaluated parameters were found to be significant as interaction effect parameters. Material type was significant as an interaction effect with raster width, amount of inner layers, and infill pattern. Raster width was significant as an interaction with the sample thickness and infill pattern. Lastly, raster angle was significant as an interaction term with infill pattern.

Furthermore, it was determined that five of the six main effects were significant in predicting flame time: material type, raster width, raster angle, number of inner layers, and infill percent. Notably, infill pattern was not included as a significant parameter for predicting flame time. In addition to the main effects, it was determined that there were several significant interaction terms that impacted flame time, including; material and raster width, material and raster angle, and material and infill percentage.

3.2.2 Zero layer

For the zero layer samples (0.02-inches-thick without any "infill" layers), it was determined that material was a significant main effect parameter in predicting burn length. Raster width was also significant as an interaction term with material. Therefore, material and raster width were significant in predicting burn length for the zero-layer sample data; raster angle was determined not to be significant.

For flame time, it was determined that material was significant in predicting flame time. Additionally, raster angle was significant in predicting flame time as a quadratic term. This means that as the raster angle increased, flame time would experience quadratic growth.

3.2.3 Generated "best" and "worst" case scenarios

From the provided DOE data, ten "worst case" and "best case" scenarios were generated to maximize or minimize the predicted burn length and flame time for each material. Within these scenarios generated, the following ranges were selected:

- Infill Pattern (None, Sparse, Sparse Double Dense (DD))

- Raster Width (0.016 inches to 0.030 inches, increments of 0.002 inches)

- Raster Angle (45° to 100°, increments of 7.5°)

- Inner Layers (0, 4 to 11, increments of 1)

- Infill Percentage (0%, 20% to 60%, increments of 10%)

All combinations were considered within the selected range. The ten combinations for maximization of the PEI-PC material blend is shown below in Table 2. The combinations for the other material types are shown within the Appendix A.

Table 2. Ten Combinations to maximize flammability data – PEI-PC blend

Rank	Predicted Burn Length [in]	Predicted Flame Time [s]	Infill %	Infill Pattern	# of Inner Layers	Raster Angle [°]	Raster Width [in]
			PEI-PC Blend				
1	0.90	4.38	0	None	0	90.0	0.016
2	0.73	4.33	0	None	0	45.0	0.016
3	0.87	3.41	0	None	0	82.5	0.016
4	0.79	3.73	0	None	0	90.0	0.018
5	0.56	4.78	0	None	0	45.0	0.030
6	0.76	3.38	0	None	0	52.5	0.016
7	0.49	4.83	0	None	0	90.0	0.030
8	0.67	3.68	0	None	0	45.0	0.018
9	0.85	2.88	0	None	0	75.0	0.016
10	0.70	3.34	0	None	0	90.0	0.020

As shown above, it was found that all "worst case" combinations for all materials were composed of 0 inner layer (0.02-inch thick) samples. This was consistent with previous testing, as it was generally observed that thinner samples produced higher measurements in recorded data. Although 0 layer samples were found to consistently increase flammability, no clear trend was observed between the raster width and raster angle parameters.

Furthermore, the ten combinations to minimize burn length and flame time of the PEI-PC material blend is displayed below in Table 3.

Table 3. Ten Combinations to minimize flammability data – PEI-PC blend

| | | | | PEI-PC Blend | | | |
Rank	Predicted Burn Length [in]	Predicted Flame Time [s]	Infill %	Infill Pattern	# of Inner Layers	Raster Angle [°]	Raster Width [in]
1	0.11	0.00	60	Sparse	11	90.0	0.016
2	0.11	0.00	60	Sparse	11	82.5	0.016
3	0.13	0.00	50	Sparse	11	90.0	0.016
4	0.12	0.00	60	Sparse	11	90.0	0.018
5	0.11	0.00	60	Sparse	11	90.0	0.016
6	0.13	0.00	50	Sparse	11	75.0	0.016
7	0.15	0.00	40	Sparse	11	82.5	0.016
8	0.12	0.00	60	Sparse	10	90.0	0.016
9	0.13	0.00	60	Sparse DD	11	90.0	0.016
10	0.11	0.00	60	Sparse	11	82.5	0.018

It was observed that samples with larger numbers of inner layers and higher infill percentages were more common within these generated values. The generated scenarios for all materials with the exception of one combination was observed to have 11 inner layers. Similarly, most of the combinations to minimize flammability data were of the higher range of the infill percentage. Within these combinations, the raster width and raster angle values to minimize flammability data varied. However, unlike the maximization combinations, the raster width and angle would vary between materials. For example, a raster width of 0.016 inches was by far the most prevalent value to appear for the PEI-PC and PES materials. Conversely, the most common raster width for the PEI and PEKK material was 0.030 inches. This observation was true for the infill pattern as well.

VBB testing was conducted to determine the validity of the maximization/minimization models. VBB tests were conducted on three of the top ten min/max scenarios for each material. Comparisons between the average recorded data and the generated data is shown in Table 4.

Similar data averages were observed compared to the generated "best" and "worst" case scenarios, reinforcing the validity of the generated scenarios.

Table 4. Generated data compared to tested data

Material	Min/Max	Data Averages		Generated Data	
		Burn Length	Flame Time	Burn Length	Flame Time
	[Rank]	[in]	[s]	[in]	[s]
PEI-PC	Min 1	0.10	0.15	0.11	0.00
	Min 2	0.10	0.00	0.11	0.00
	Min 3	0.10	0.00	0.13	0.00
PES	Min 1	0.10	1.33	0.08	0.86
	Min 2	0.10	0.85	0.08	0.86
	Min 3	0.10	1.33	0.08	0.86
PEI	Min 1	0.10	0.00	0.08	0.00
	Min 2	0.10	0.00	0.08	0.00
	Min 3	0.10	0.25	0.08	0.00
PEKK	Min 1	0.10	0.00	0.11	0.01
	Min 2	0.10	0.00	0.10	0.01
	Min 3	0.10	0.33	0.10	0.02
PEI-PC	Max 1	0.75	4.45	0.90	4.38
	Max 2	0.65	3.18	0.73	4.33
	Max 3	1.28	10.45	0.87	3.41
PES	Max 1	4.00	98.90	4.20	112.74
	Max 2	4.00	122.00	4.02	114.72
	Max 3	4.00	108.23	4.11	107.65
PEI	Max 1	0.40	4.68	0.53	4.84

Material	Min/Max	Data Averages		Generated Data	
		Burn Length	Flame Time	Burn Length	Flame Time
	[Rank]	[in]	[s]	[in]	[s]
	Max 2	0.35	3.18	0.46	4.90
	Max 3	0.38	3.20	0.52	3.84
PEKK	Max 2	0.23	3.10	0.29	6.07
	Max 4	0.35	5.35	0.34	4.88
	Max 6	0.38	7.70	0.24	6.13

4   Conclusion

All evaluated parameters were found to have some significance on the impact on the flammability of a 3D printed part. It was observed throughout testing that three of the tested parameters (material type, infill percentage, and sample thickness) had the largest impact on burn length, flame time, and drip flame time. Generally speaking, the material type and the amount of material itself were factors that were found to produce the largest effect on flammability. Other parameters, such as raster width, raster angle, infill pattern, and print orientation were observed to produce only interaction effects in conjunction with the other print variables listed. Furthermore, alterations in these parameters were observed to produce more variability in recorded data at lower infill percentages.

In order to get a comprehensive understanding of the relationship between flammability and the parameters used during the production process of a 3D printed part, additional testing may be needed. Specifically, an analysis on samples produced from other AM methods besides FFF may be needed to determine if changes in production methods impact the results observed within this study. Furthermore, additional parameters used throughout the production process will need to be evaluated to ensure an adequate understanding of the relationship between the parameters utilized within an AM process and the flammability of a 3D printed part.

5   References

3D printing technology is now taking on airplane interiors. (2017, April 4). Retrieved from 3D
    Natives: https://www.3dnatives.com/en/3d-printed-plane-part040420174/#!

FAA. (2023, November 11). *Aircraft Materials Fire Test Handbook*. Retrieved from
    https://www.fire.tc.faa.gov/Handbook

GAO. (2015). *3D Printing - Opportunities, challenges, and policy implications of additive
    manufacturing.* United States Government Accountability Office.

Grand View Research. (n.d.). *Additive manufacturing market size, share & trends analysis
    report*. Retrieved from Grand View Research:
    https://www.grandviewresearch.com/industry-analysis/additive-manufacturing-market

Joshi, S. C., & Sheikh, A. A. (2015). *3D printing in aerospace and its long-term sustainability.*
    Nanyand Technological University.

Mokalled, S., & Basu, S. (2022). *Bunsen burner flammability analysis.* Boeing.

Molitch-Hou, M. (2018, April 12). *Airbus to install first 3-D printed components into aircraft
    cabins*. Retrieved from https://www.engineering.com/story/airbus-to-install-first-3d-
    printed-components-into-aircraft-cabins

National Archives and Records Administration. (2023, November 9). *25.853 Compartment
    interiors*. Retrieved from Code of Federal Regulations:
    https://www.ecfr.gov/current/title-14/chapter-I/subchapter-C/part-25/subpart-D/subject-
    group-ECFR1e1f52030ba4797/section-25.853

A   Bunsen burner flammability analysis

Bunsen Burner Flammability Analysis

Stefani Mokalled, Shobbo Basu

Report Date: 7/1/2022

Table of Contents

Introduction

The team that was a part of this analysis was

Federal Aviation Administration:
Steve Rehn
Dan Keslar
Boeing:
Yaw Agyei – Flammability

Genya Shimada – Flammability
Brian Johnson – Flammability
Elizabeth Rusch-Franck – Flammability
Stefani Mokalled – Applied Mathematics
Shobbo Basu – Applied Mathematics

This analysis was completed on the data from the Bunsen Burner flammability experiment. The original data set consists of 480 data observations. There were 120 unique experimental runs, with 4 replicates per experiment. The responses of interest are the burn length (in), flame time (s), dripping (yes/no if dripping occurred), and drip flame time (s). The burn lengths were measured with a ruler to the nearest 0.1 inch after witnessing the test (8 inches for failure on 12-second test, 6 inches for 60-second test). The flame times were measured with a stop watch to the nearest 0.1 second by the operator of the test (15 seconds for failure on both tests). The drip flame time were measured with a stop watch to the nearest 0.1 second by the operator of the test (5 seconds for failure on 12-second test, 3 seconds for 60-second).

We considered the significance of material type, Raster Width (0.030, 0.022, 0.018, and 0.016 inches), Raster Angle (90, 67.5, and 45.0 degrees), Inner Layers (11, 4, and 0), Infill Percentage (100%, 20%, 60%, and 0%), and Infill Pattern (Sparse, Sparse DD, Hexagram, and None) in relation to the response variables. Note that there were four material types: Polyetherimide/Polycarbonate Blend (PEI-PC), Polyetherimide (PEI), Polyethersulfone (PES), Polyetherketoneketone (PEKK). The following figures provide pictures of the different factors considered in the experiment.

Figure 1 presents the different material types that were considered in the study.

Figure 1: Material Types

Figure 2 presents the different raster widths. The thickness of the extruded inner material increases from left to right, although this is a difficult to see in the pictures and is not visible in the samples.

0.016" Width   0.018" Width   0.022" Width   0.030" Width
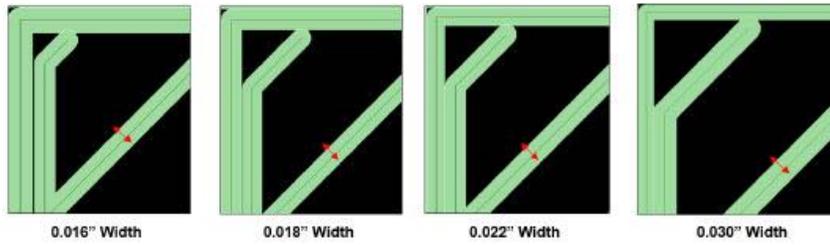
Figure 2: Raster Width

Figure 3 presents the different raster angles. We see the angles changing in the pictures and samples as we move from left to right.

45° Angle   67.5° Angle   90° Angle
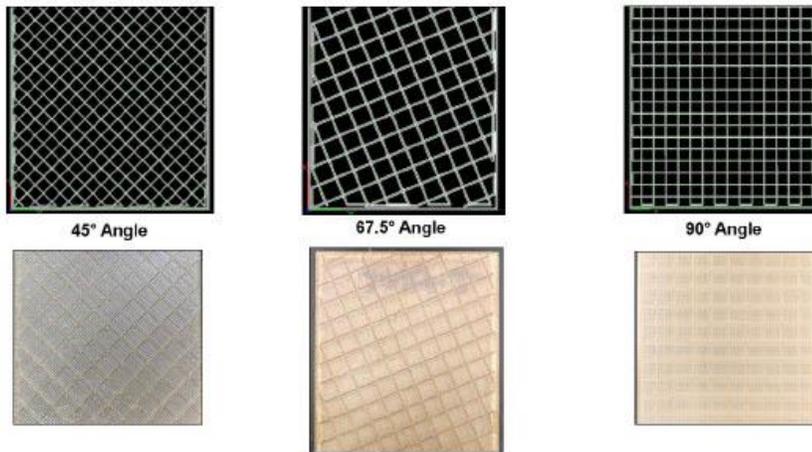
Figure 3: Raster Angle

Figure 4 presents the different number of inner layers. We see that the thickness increases by 0.06" going from 0 to 4 inner layers, and by 0.07" going from 4 to 11 inner layers.

| 0 Inner Layers | 4 Inner Layers | 11 Inner Layers |
| 0.02" Thick | 0.08" Thick | 0.15" Thick |
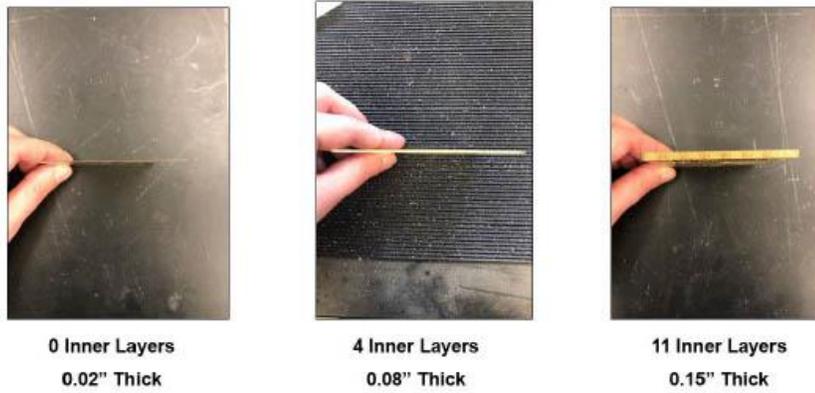
Figure 4: Inner Layers

Figure 5 presents the different infill percentages. We can see more infill as infill percentage increases in the pictures, although this is not visible in pictures of the actual samples.
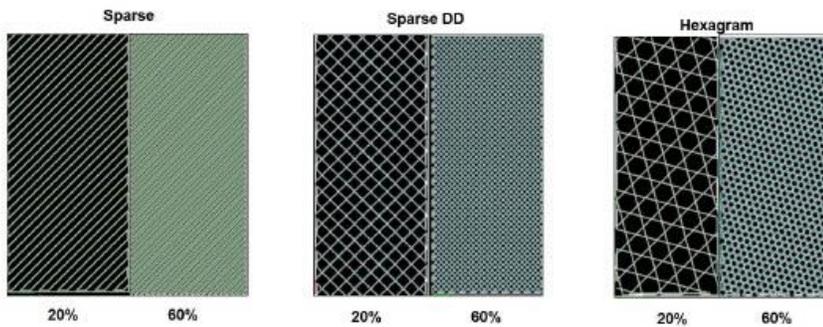
Figure 5: Infill Percentage

Figure 6 presents the different infill patterns. Here we see the differences in the patterns of the infill in moving from left to right.
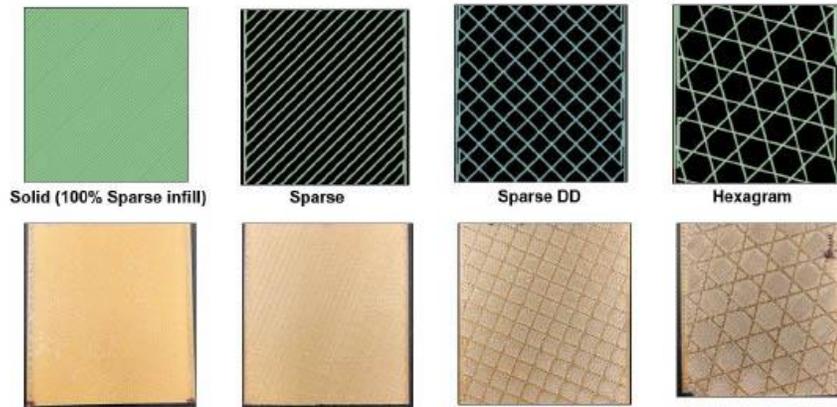
Figure 6: Infill Pattern

Figure 7 presents differences in burn lengths, post testing.
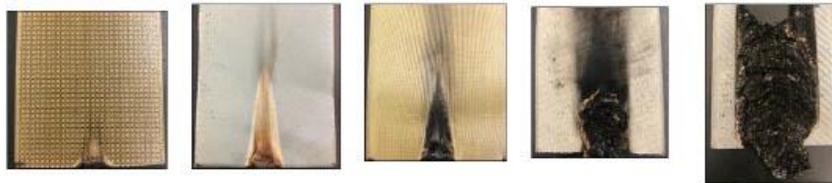
Figure 7: Burn Lengths Post Testing

Note that there do not exist observations for each experimental combination of factors. The 0 inner layer tests only consider material, raster width, and raster angle as variables since the infill percentage is only 0% and the infill pattern is only None when inner layer is 0. Due to printing constraints, some combinations of factors could not be completed. For example, all 0.016", 0.018", and 0.022" raster width 60% infill Hexagram samples were removed from the experiments, leaving only 20% infill for the Hexagram pattern. Additionally, all PEKK 0.016" raster width samples were changed and completed at 0.018" instead. Lastly, the 100% infill percentage was only possible for the Sparse pattern (technically the 100% infill pattern is the same as the sparse pattern but with no gaps between the rasters), and not for Hexagram or Sparse DD.

To proceed with the data analysis, we focused on the portion of the data in which all experiments were completed. In this analysis, the 100% infill percentage experiments were removed (since these only consisted of the Sparse infill pattern). All Hexagram samples were also removed from the analysis due to the limited data on this infill pattern (only 20% infill observations). The PEKK 0.018" experiments for the zero layer data were also removed since these observations were outliers compared to the remaining experiment results for the zero layer data. Lastly, the PEKK 0.018" experiments for the nonzero layer data were coded as

0.016", as they were not significantly different than other observations and could be considered with the 0.016" observations. This leaves 332 observations for analysis (224 for nonzero layer data and 88 for zero layer data). To complete model fitting, all burn lengths and flame times were shifted by 0.1 to avoid numerical issues close to and at 0. The predicted values were then shifted back by 0.1 to adjust back to the original scale. Lastly, note that 23 of the burn lengths were recorded as >4.0; all of these observations were set to burn length 4.0 for analysis.

In terms of the data, although in general burn lengths and flame time increase together, there were some instances in which the burn length went up very quickly and came back down. This resulted in a high burn length with a short flame time. This can be seen in the following plot of burn length vs. flame time.

Burn Length vs. Flame Time
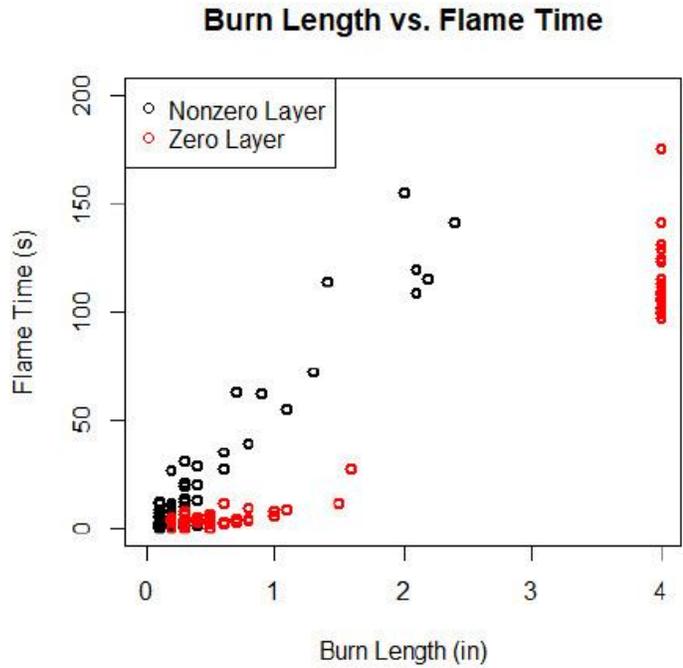
From the preceding plot,

All observations with the burn length of 4.0 (or more) have PES material with 0 inner layers.

A few observations have longer burn lengths with short flame times. These are mostly PEI-PC material with 0 inner layers.

Since some of the data was removed from the analysis (specifically, the 100% infill percentage data and the Hexagram data), two smaller follow-up analyses were also completed to draw conclusions on the remaining observations. In particular, one analysis was completed on the Sparse only data since this contains the 100% infill percentage information. A second analysis was completed on the 20% data since this contains the Hexagram data. These analyses contain only the nonzero layer data, so model fitting was completed for the nonzero burn length and nonzero flame time for these data subsets.

In what follows, all the plots and observations are provided on the main analysis (the data without the 100% infill percentage and without the Hexagram infill pattern). In Section 2, we check for consistency in the data. In Section 3, we complete analysis and regression modeling for the burn lengths for the nonzero layer data (in Section 3.1) and zero layer data (in Section 3.2). Conclusions based on the follow-up analyses are provided in Section 3.1.1. In Section 4, we complete analysis and regression modeling for the flame time for the nonzero layer data (in Section 4.1) and zero layer data (in Section 4.2). Conclusions based on the follow-up analyses are provided in Section 4.1.1. In Section 5, we analyze the occurrence of dripping in the data to determine which factors are significant in predicting dripping. In Section 6, we provide the optimal combinations that minimize and maximize burn length and flame time by material type, with some discussion on conditions that minimized/maximized burn length and flame time for the follow-up analysis. We end with a conclusion of the results in Section 7.

Data Consistency

We begin by studying the consistency in the data. The following is a plot of the standard deviations of the burn length for each experiment.

Standard Deviations of Burn Lengths by Experiment
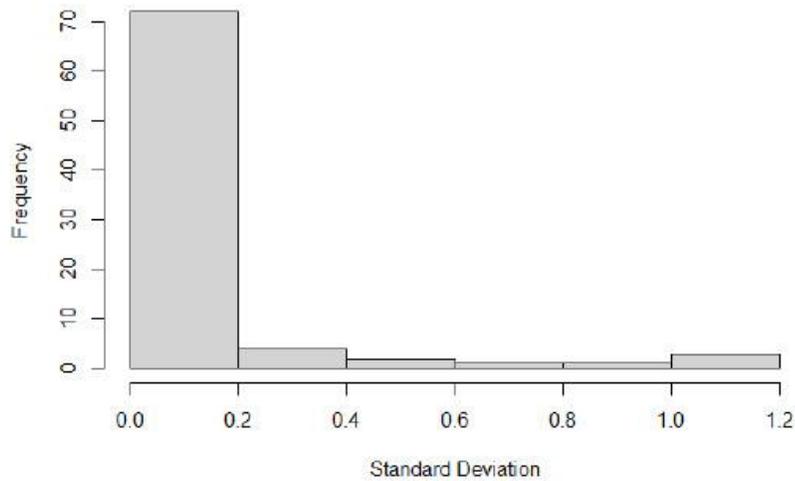
From the plot,

The largest frequency of the experiments have burn length standard deviations less than 0.4in. Burn length standard deviations vary to 1.2in.

The data is generally consistent, with a few observations having more variability in their burn lengths.

The experiments with standard deviations larger than 0.4in are all PES material, with the exception of one experiment with PEI-PC.

These experiments vary in terms of raster width, raster angle, inner layers, infill percentage, and infill pattern.

The following is a plot of the standard deviations of the flame times for each experiment.

Standard Deviations of Flame Times by Experiment
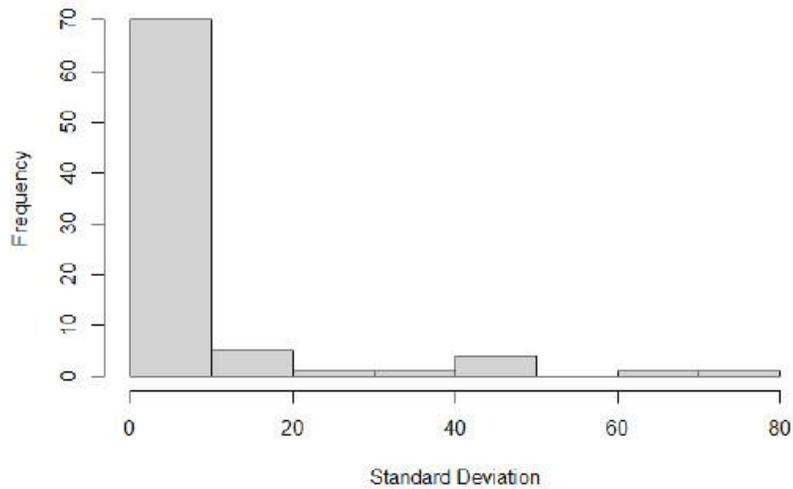
From the plot,

The largest frequency of the experiments have flame time standard deviations less than 20 s. Flame time standard deviations vary to 80 s.

The data is generally consistent, with a few observations having more extreme flame times, similar to the burn length observations.

The experiments with standard deviations larger than 20 s are all PES material.

These experiments also vary in terms of raster width, raster angle, inner layers, infill percentage, and infill pattern.

Almost all of the experiments with large burn length standard deviations also have large flame time standard deviations.

Burn Length Model

To begin modeling the burn lengths, we first study plots of the covariates versus the burn length for the data.
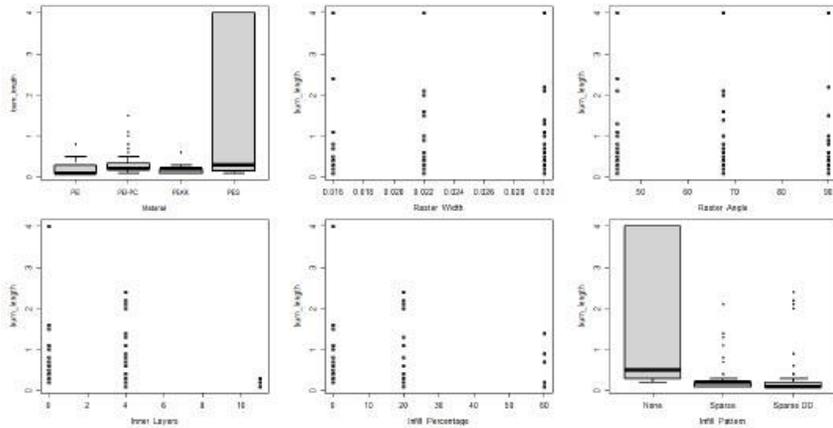
From the plots,

It appears that PES has the highest burn length of the four materials with the greatest amount of variability, with PEI-PC having the next greatest variability and burn length values.

The three raster width and raster angles have similar amounts of variability and burn length.

The zero layer data result in the highest burn length (>4.0), with the largest amount of variability.

The burn length appears to decrease as number of inner layers increases, with the 11 layer data having the smallest burn length.

Additionally, it appears that infill percentage may be quadratically related to the burn length, with a large infill percentage resulting in shorter burn lengths.

The infill pattern None (no infill) leads to the greatest variability in burn lengths, with the highest burn length of the four infill patterns. Note that this infill pattern corresponds only to the zero layer data with 0% infill percentage.

Next, we look at the 2-way interaction effects of the covariates versus the burn length.
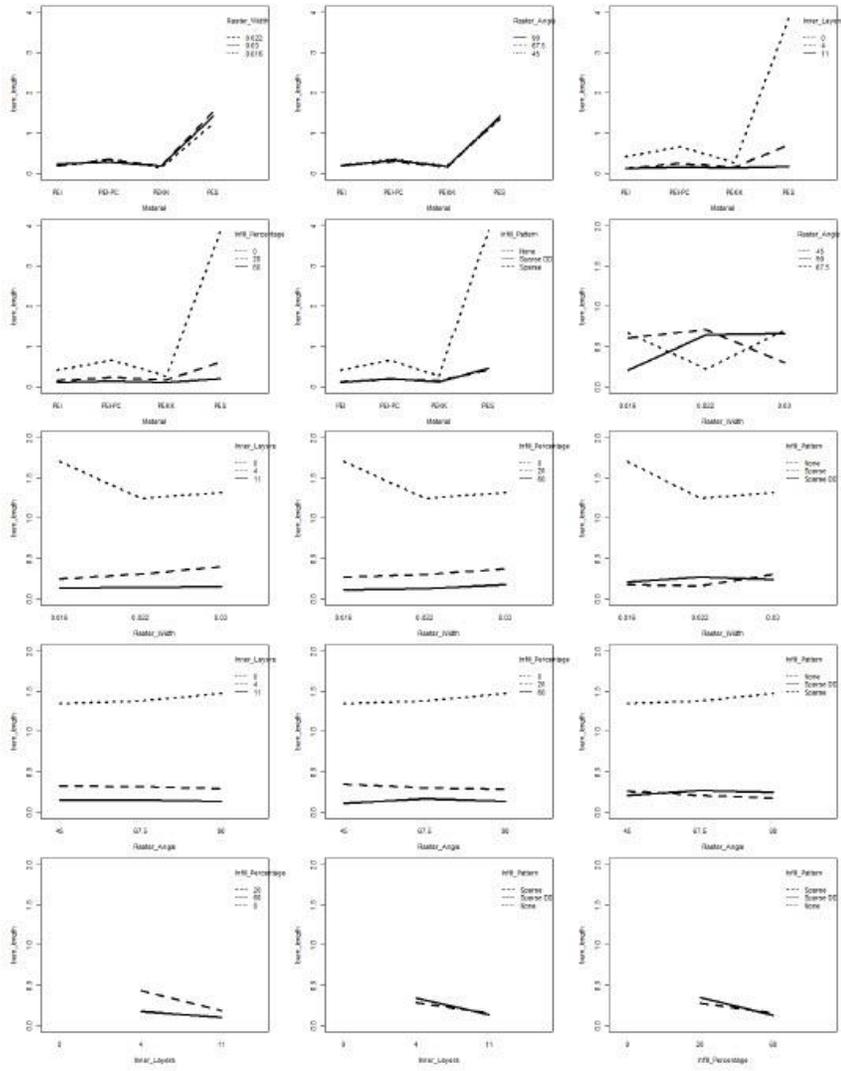
From the plots,

It appears that an interaction effect exist for many of the variables. That is, the effect of a variable on the burn length depends on the level of another variable.

For example, there seems to be an interaction effect for material and inner layers, with the 0 layer PES data having higher burn lengths than the other material.

Similarly, there seems to be an interaction effect between material and infill percentage specifically for PES, with the 0% having a higher burn length than the other materials.

Material also seems to have an interaction effect with infill pattern, with the None pattern for PES having a higher burn length than the other material types.

Raster width also appears to have interaction effects with raster angle, inner layers, infill percentage, and infill pattern.

Lastly, there appears to be interaction effects between inner layers and infill percentage, inner layers and infill pattern, and infill percentage and infill pattern.

To proceed with model fitting, we divide the data into nonzero and zero layer data since we do not have observations for all possible experiment combinations (e.g., there are no nonzero layer observations for the infill pattern none). Since the data do not look normally distributed, we investigate power transformations of the burn lengths.
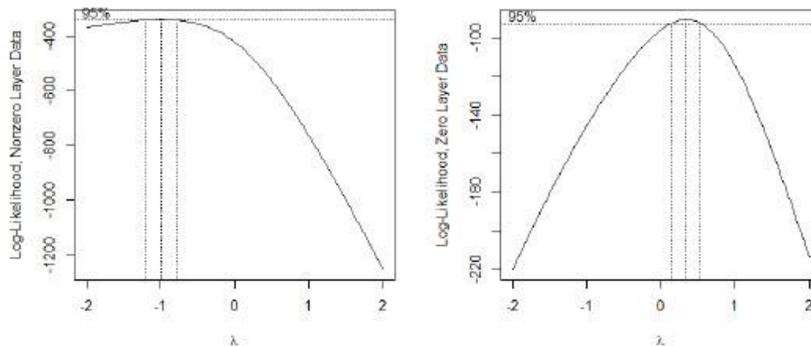
Since the λ parameter for the nonzero layer data (left) is close to -1, we conclude that an inverse transformation of burn length is needed to transform the data for normality.

Since the λ parameter for the zero layer data (right) is close to 1/2, we conclude that a square root transformation of burn length is needed to transform the data for normality.

In the following sections, we fit models to the inverse of the burn length for nonzero layer data, and square root of burn length for the zero layer data. Note that in discussing the significant factors in the model, a significance level of 0.1 is used. That is, a variable with a p-value on the coefficient that is less than 0.1 is considered significant. This significance level can be decreased as needed.

Nonzero Layer Data

To fit the inverse burn length model, we use forward and backward step AIC (Alkaline Information Criterion) for variable selection. The algorithm is allowed to choose from all six main effects, the square of the continuous variables (raster width, raster angle, infill pattern, infill percentage), and all 2-way interaction effects. The procedure adds and removes variables from the model to minimize the AIC, which is a measure of goodness of fit of a regression model. The following is the summary of the model fit.

term	df	sumsq	meansq	statistic	p.value
Material	3	78.9649303	26.3216434	67.0130161	0.0000000
Raster_Width	1	3.7157484	3.7157484	9.4600290	0.0023686
Raster_Angle	1	0.0000631	0.0000631	0.0001606	0.9899009
Inner_Layers	1	40.6592162	40.6592162	103.5154478	0.0000000
Infill_Percentage	1	100.7995590	100.7995590	256.6284465	0.0000000
Infill_Pattern	1	1.5144473	1.5144473	3.8556743	0.0508493
I(Raster_Angle^2)	1	0.5829090	0.5829090	1.4840446	0.2244596
Material:Raster_Width	3	4.2261669	1.4087223	3.5865059	0.0145831
Material:Raster_Angle	3	1.5530594	0.5176865	1.3179926	0.2693995
Material:Inner_Layers	3	23.7529061	7.9176354	20.1577317	0.0000000
Material:Infill_Percentage	3	6.5194919	2.1731640	5.5327195	0.0011164
Raster_Width:Inner_Layers	1	1.6091767	1.6091767	4.0968485	0.0441833
Raster_Width:Infill_Percentage	1	0.5571951	0.5571951	1.4185787	0.2349327
Raster_Width:Infill_Pattern	1	2.1790176	2.1790176	5.5476224	0.0193934
Raster_Angle:Infill_Pattern	1	2.4296995	2.4296995	6.1858406	0.0136276

Residuals	218	85.6269216	0.3927840	NA	NA

The adjusted R^2 of this model is 0.73, indicating a reasonable fit of the model to the data.

From the preceding analysis, we determine that five of the six main effect variables (material type, raster width, inner layers, infill percentage, and inner pattern) are significant, given the other variables are in the model.

This reflects what was found in the initial plots of covariates versus burn lengths.

Several variables are also significant as interaction effect variables:

Material is significant as an interaction effect with raster width, inner layers, and infill percentage.

Raster width is significant as interaction with inner layers and infill pattern.

Raster angle is significant as an interaction term with infill pattern.

These significant interaction effects were also seen in the analysis of the interaction plots.

Hence, all six variables are significant as either main effect or interaction effect variables in predicting burn length for the nonzero layer data. Although raster angle is not significant as a main effect variable, it is significant as an interaction effect.

We next create diagnostic plots to study the appropriateness of the model.
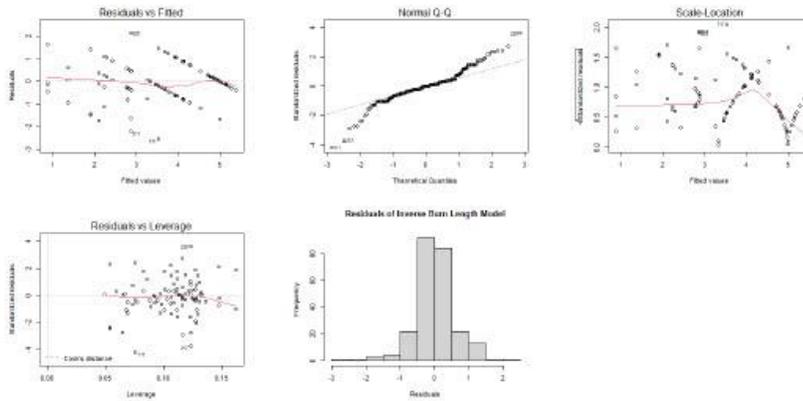
It appears the normality assumption is satisfied in fitting the regression model (from checking the QQ plot and the histogram of residuals).

Although the residual plots do demonstrate some patterns, upon further study we determined that this is due to the data itself.

Since the observations were rounded to the nearest 0.1 inch, several of the observed burn lengths are of the same value. However, the fitted values of these observations differ, and, hence, the differences result in a trend.

The following are plots of the covariates versus the residuals.
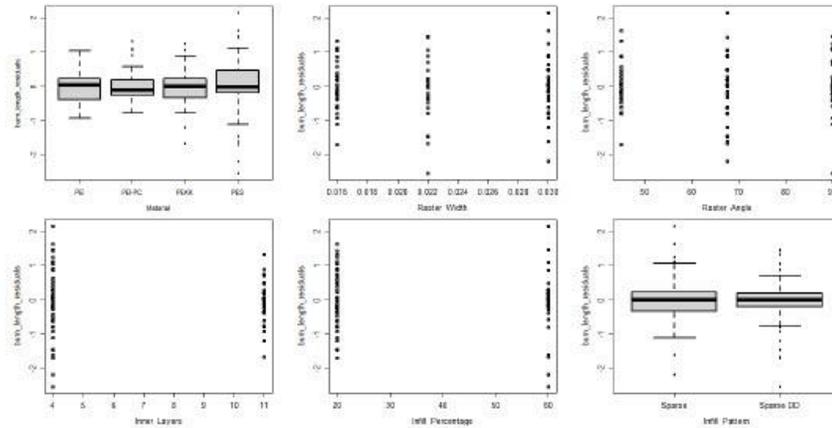
Since the residuals are scattered evenly around 0, the model fit seems appropriate.

Lastly, we create plots of the actual vs. fitted burn lengths as well as the average of the actual and fitted burn lengths (for each experiment group).

Burn Length Actual vs. Fitted   **Average Burn Length Actual vs. Fitted**
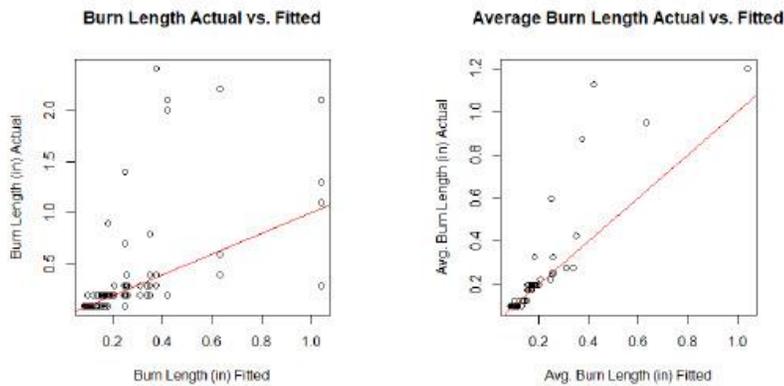
From the plots,

We see that the actual vs. fitted values follow a generally linear trend, in particular for the averages in which the variability has been removed. This indicates that the model is performing well in predicting the actual burn length values.

However, there are a handful of observations (around 4 observations) which fall outside of the linear trend.

Specifically, these observations are all PES material with 4 inner layers, and variations in the other variables (raster width, raster angle, infill percentage, and infill pattern).

Followup Analysis

For the Sparse infill pattern only model in which the 100% infill percentage was considered in the data, we found the following variables are significant in the model:

Material
Raster width
Raster angle
Infill percentage
Inner layers
Raster angle squared
Infill percentage squared
Interaction effects:
Material and raster width, raster angle, infill percentage,inner layers
Raster width and raster angle, inner layers
Raster angle and infill percentage
Infill percentage and inner layers

The significant squared terms indicate a quadratic relationship between the factor and the burn length rather than a linear relationship.

For the 20% infill percentage only model in which the Hexagram infill pattern was considered in the data, we found the following variables are significant in the model:

Material
Inner layers
Interaction effects:
Material and inner layers
Raster width and infill pattern
Raster angle and infill pattern
Inner layers and infill pattern

Note that infill pattern is not a factor for the Sparse only model, and infill percentage is not a factor for the 20% only model. Hence, all variables are significant as either main or interaction effect variables for both the Sparse only and 20% only models as well. Therefore, we conclude that all six variables are significant in predicting burn length for the nonzero layer data.

Zero Layer Data

To fit the square root of burn length model, we used forward and backward step AIC for variable selection as detailed previously. The algorithm is allowed to choose from the three main effects, the square of the continuous variables (raster width and raster angle), and all the 2-way interaction effects. The following is the summary of the model fit.

term	df	sumsq	meansq	statistic	p.value
Material	3	28.2809384	9.4269795	590.4818288	0.0000000
Raster_Width	1	0.0029932	0.0029932	0.1874847	0.6662288
Raster_Angle	1	0.0040643	0.0040643	0.2545800	0.6153093
I(Raster_Width^2)	1	0.0292084	0.0292084	1.8295389	0.1801408
Material:Raster_Width	3	0.1147605	0.0382535	2.3961004	0.0746125
Raster_Width:Raster_Angle	1	0.0313952	0.0313952	1.9665141	0.1648372
Residuals	77	1.2292968	0.0159649	NA	NA

The adjusted R^2 of the model is 0.95, indicating a great fit of the model to the data.
From the preceeding analysis, we determine that material type is the significant main effect variable, given the other variables are in the model. This was reflected in the initial data plots.

Raster width is also significant as an interaction term with material.
For the zero layer data, two of the three factors (material and raster width) are significant in predicting burn length.

We next create diagnostic plots to study the appropriateness of the model.
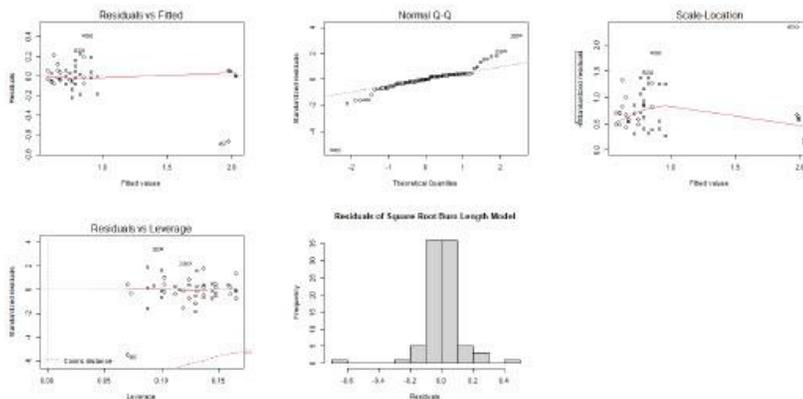
It appears the normality assumption is satisfied in fitting the regression model (from checking the QQ plot and the histogram of residuals).

Although the residual plots do demonstrate some patterns, upon further study we determine that this is due to the data itself.

The randomness of the residual plots is impacted due to several extreme observations; in particular, for burn lengths that are 4.0 in. (as set for model fitting, although these were measured as >4.0 in the data set).

The following are plots of the covariates versus the residuals.
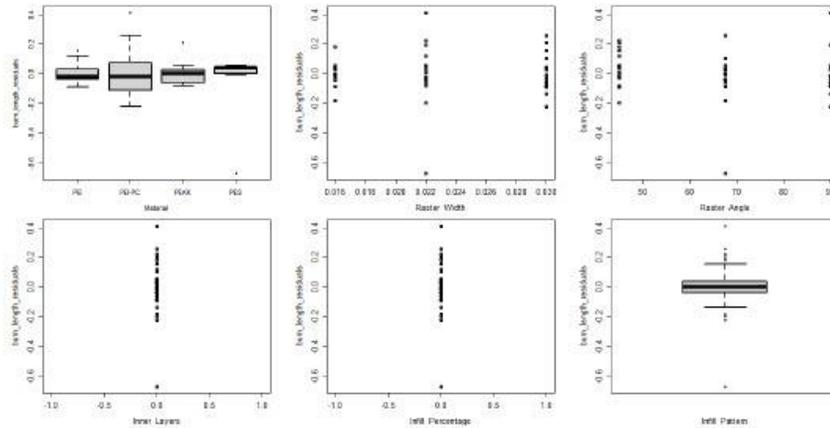
Since the residuals are generally scattered evenly around 0, the model fit seems appropriate.

Lastly, we create plots of the actual vs. fitted burn lengths as well as the average of the actual and fitted burn lengths (for each experiment group).
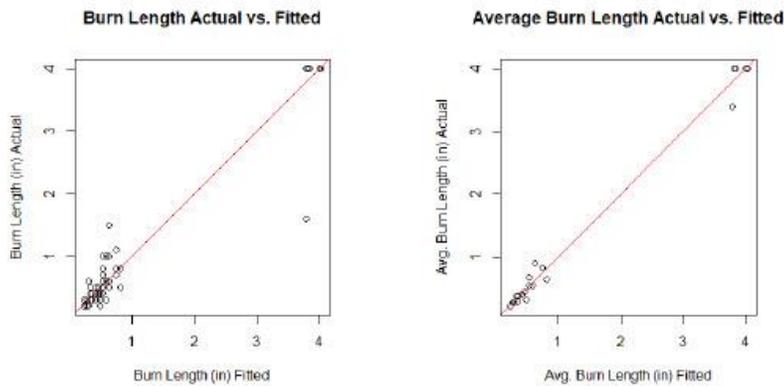
From the plots,

We see that the actual vs. fitted values follow a generally linear trend, in particular for the averages in which the variability has been removed.
This indicates that the model is performing well in predicting the actual burn length values.

Flame Time Model

To begin with modeling the flame time, we first study plots of the covariates versus the flame time for the data.
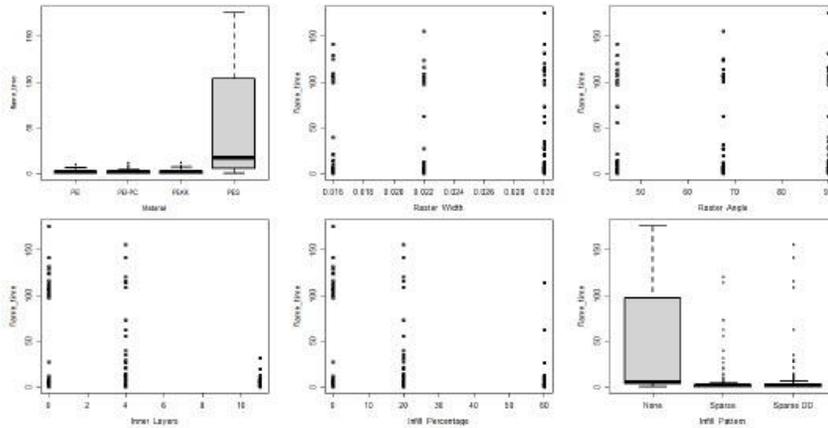
From the plots,

It appears that PES has the longest flame time of the four materials with the greatest amount of variability.

The flame time appears to increase slightly with raster width, with raster width of 0.03" having the highest flame time and greatest variability.

The flame time also seems to increase slightly with raster angle, with the 90 degree angle having the most variability and longest flame time.

The flame time decreases with number of inner layers, with the zero layer data result in the longest flame time, with the largest amount of variability.

Additionally, it appears that flame time decreases with infill percentage, with a large infill percentage resulting in shorter flame time.

Finally, the infill pattern None (no inner layers) leads to the greatest variability in flame time, with the longest flame time of the three infill patterns.

We next look at the 2-way interaction effects of the covariates versus the flame time.
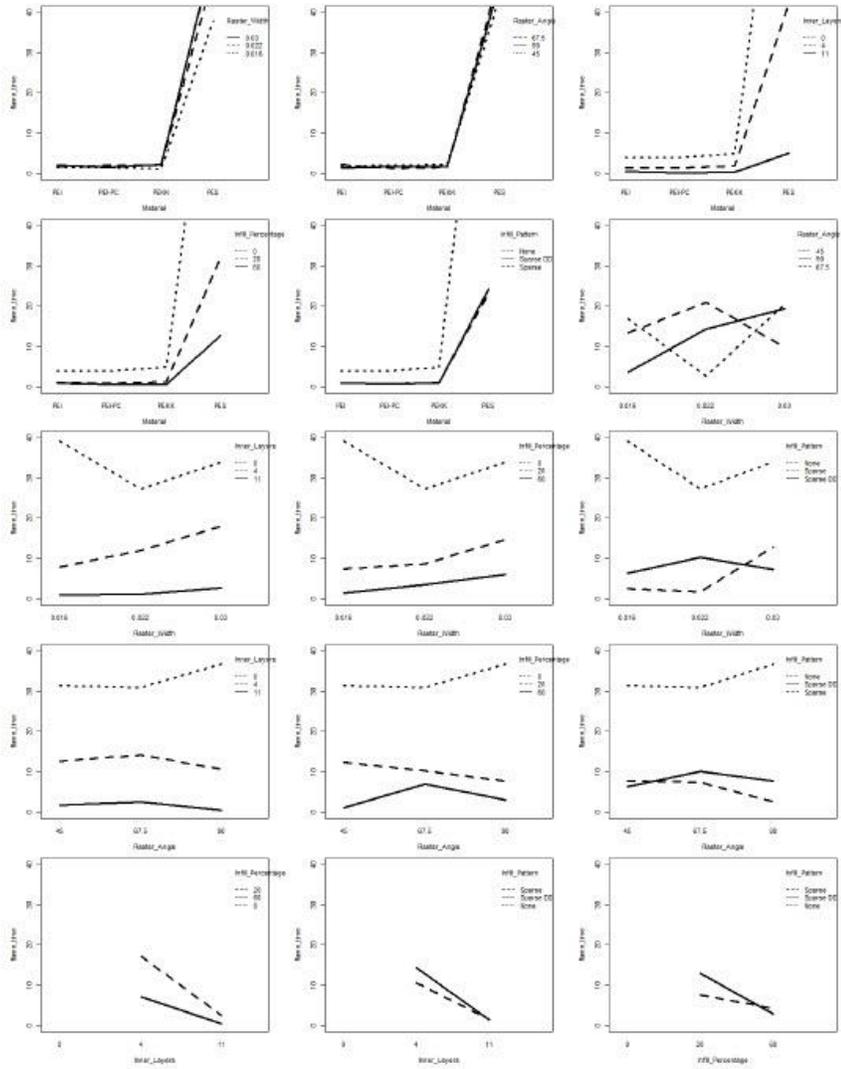
From the

plots,

There appears to be interaction effects between many of the variables, as was the case for the burn length plots. That is, the effect of a variable on the flame time depends on the level of another variable.

For example, the mean flame time for the PES material differs based on different levels of raster width, inner layers, infill percentage, and infill pattern.

Additionally, the mean flame time appears to differ for raster width given different levels of raster angle, inner layers, infill percentage, and inner pattern.

The mean flame time for the raster angle seems to differ depending on inner layers, infill percentage, and infill pattern.

Lastly, there also appear to be an interaction effect between inner layers and infill pattern as well as infill percentage and infill pattern.

To proceed with model fitting, we divide the data into nonzero and zero layer data, as was done for the burn length data. Since the data do not look normally distributed, we investigate power transformations of the flame time.
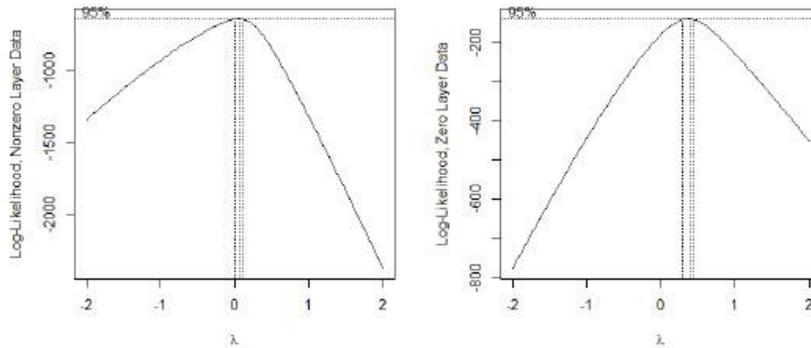
Since the λ parameter for the nonzero layer data (left) is close to 0, we conclude that a logarithmic transformation of flame time is needed to transform the nonzero layer data for normality.

Since the λ parameter for the zero layer data (right) is close to 1/2, we conclude that a square root transformation of flame time is needed to transform the data for normality.

In the following sections, we fit models to the log of the flame time data for nonzero layer data, and square root of flame time data for the zero layer data.

Nonzero Layer Data

To fit the log of flame time model, we use forward and backward step AIC for variable selection. The algorithm is allowed to choose from the six main effect variables, the square of the

continuous variables (raster width, raster angle, inner layers, and infill percentage), and all 2-way interaction effects. The following is the summary of the model fit.

term	df	sumsq	meansq	statistic	p.value
Material	3	405.1333930	135.0444643	152.3208423	0.0000000
Raster_Width	1	2.8698035	2.8698035	3.2369404	0.0733530
Raster_Angle	1	3.4513084	3.4513084	3.8928378	0.0497332
Inner_Layers	1	237.7673813	237.7673813	268.1852083	0.0000000
Infill_Percentage	1	17.3090998	17.3090998	19.5234709	0.0000155
Infill_Pattern	1	0.3607811	0.3607811	0.4069362	0.5241861
I(Raster_Width^2)	1	2.1252074	2.1252074	2.3970874	0.1229857
Material:Raster_Width	3	10.6023992	3.5341331	3.9862584	0.0085881
Material:Raster_Angle	3	5.6312513	1.8770838	2.1172210	0.0989042
Material:Infill_Percentage	3	8.2318469	2.7439490	3.0949852	0.0277825
Material:Infill_Pattern	3	5.2426611	1.7475537	1.9711201	0.1191889
Residuals	222	196.8205442	0.8865790	NA	NA

The adjusted R^2 of the model is 0.76, indicating a reasonable fit of the model to the data.

From the preceeding analysis, we determine that five of the six main effects are significant; material, raster width, raster angle, inner layers, and infill percentages are the significant main effect variables, given the other variables are in the model.

These reflect what was seen in the main effect plots.

Significant interaction terms include:

Material and raster width.

Material and raster angle.

Material and infill percentage.

These results align with the conclusions we made based on the interaction plot analysis.

For the nonzero layer data, five of the six variables (all except infill pattern) are significant in predicting flame time.

We next create diagnostic plots to study the appropriateness of the model.
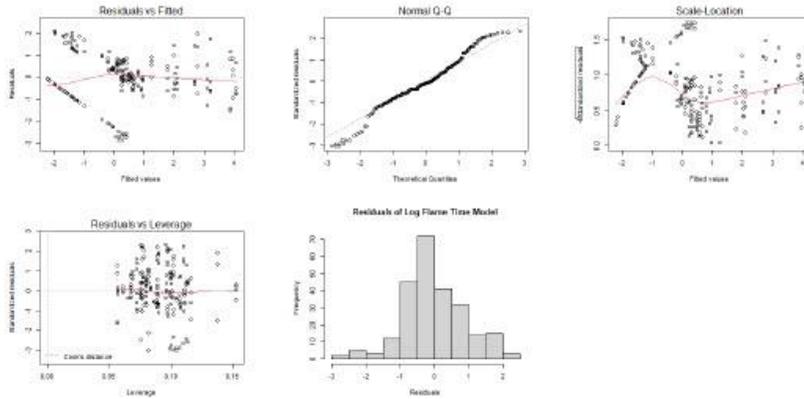
It appears the normality assumption is satisfied in fitting the regression model (from checking the QQ plot and the histogram of residuals).

Although the residual plots do demonstrate some patterns, upon further study we determine that this is due to the data itself.

Since there are several of the observed flame times that have the same value with differing fitted values, these result in a trend in the residual plots.

The following are plots of the covariates versus the residuals.
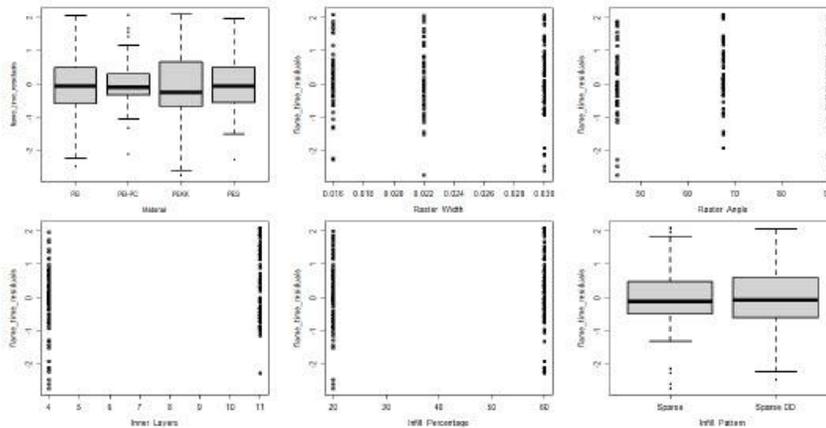
Since the residuals are scattered evenly around 0, the model fit seems appropriate.

Lastly, we create plots of the actual vs. fitted flame times as well as the average of the actual and fitted flame times (for each experiment group).

Flame Time Actual vs. Fitted   Average Flame Time Actual vs. Fitted
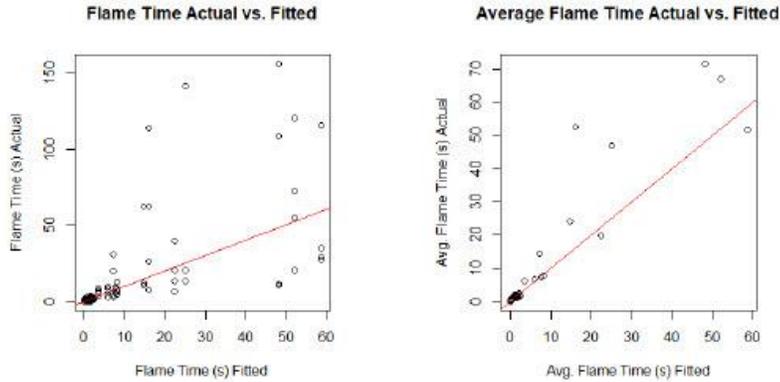
From the plots,

We see that the actual vs. fitted values follow a generally linear trend, in particular for the averages in which the variability has been removed. This indicates that the model is performing well in predicting the actual flame time values.

However, there are a handful of observations (around 4 observations) which fall outside of the linear trend.

Specifically, these observations are all PES material with 4 inner layers, with variations in the other variables (raster width, raster angle, infill percentage, and infill pattern).

These conclusions are similar to those from the nonzero burn length model.

Follow-up Analysis

For the Sparse only model in which the 100% infill percentage was considered in the data, we found the following variables are significant in the model:

Material
Raster width
Raster angle
Infill percentage
Inner layers
Raster width squared
Infill percentage squared
interaction effects:
Material and width, raster angle, infill percentage, inner layers

The significant squared terms indicate a quadratic relationship between the factor and the burn length rather than a linear relationship.

For the 20% infill percentage only model in which the Hexagram infill pattern was considered in the data, we found the following variables are significant in the model:

Material
Inner layers
Raster angle squared
Interaction effects:
Raster width and raster angle
Raster width and inner layers

Inner layers and infill pattern

Note that infill pattern is not a factor for the Sparse only model, and infill percentage is not a factor for the 20% only model. Hence, all variables are significant as either main or interaction effect variables for both the Sparse only and 20% only models. Therefore, we conclude that five of the six variables are significant in predicting flame time for the nonzero layer data across these models. Only infill pattern was not significant in the original flame time model, although it is significant in predicting flame time in the 20% only model and in predicting the burn lengths.

Zero Layer Data

To fit the square root of flame time model, we use forward and backward step AIC for variable selection as detailed previously. The algorithm is allowed to choose from the three main effect variables, the square of the continuous variables (raster width and raster angle), and all 2-way interaction effects. The following is the summary of the model fit.

term	df	sumsq	meansq	statistic	p.value
Material	3	1241.805714	413.9352381	560.0967509	0.0000000
Raster_Width	1	1.113746	1.1137460	1.5070123	0.2231955
Raster_Angle	1	0.028565	0.0285650	0.0386513	0.8446396
I(Raster_Width^2)	1	1.562572	1.5625720	2.1143199	0.1498390
I(Raster_Angle^2)	1	3.362356	3.3623557	4.5496114	0.0359915
Residuals	80	59.123391	0.7390424	NA	NA

The adjusted R^2 of the model is 0.95, indicating a great fit of the model to the data.

From the preceding analysis, we determine that material type is significant in predicting the flame time.

We also find that raster angle (squared term) is significant in predicting flame time. This indicates that as the raster angle increases, flame time increases quadratically (rather than linearly).

Two of the three variables are significant in predicting flame time for the zero layer data.

For the flame time models, we find that 5 of the 6 variables are significant in predicting flame time (all but infill pattern). For the burn length models, we found all 6 variables significant in predicting burn length, either as a main effect or interaction effect variable.

We next create diagnostic plots to study the appropriateness of the model.
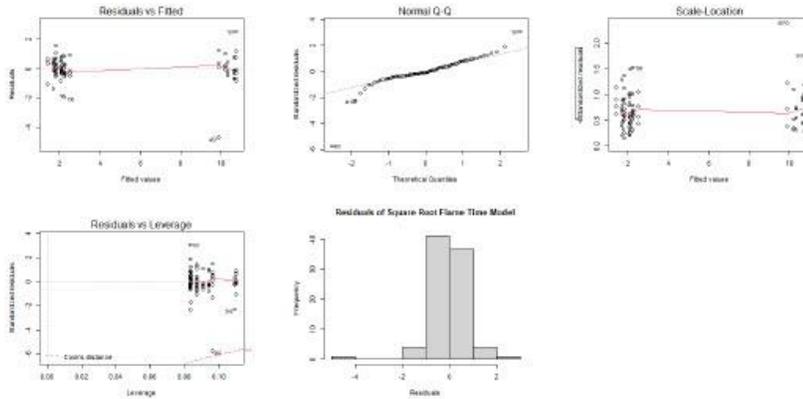
It appears the normality assumption is satisfied in fitting the regression model (from checking the QQ plot and the histogram of residuals).

The plot of the fitted values vs. the residuals is in general randomly scattered, indicating a good fit of the model.

The division in the fitted values for this plot is due to the larger actual observations.

That is, similar to the burn length residuals, the residual patterns seen here are also due to the observed data themselves.

The following are plots of the covariates versus the residuals.
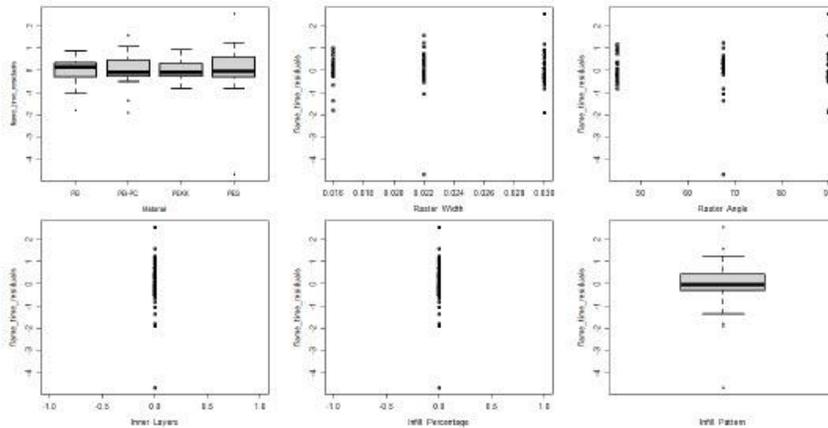
Since the residuals are scattered evenly around 0, the model fit seems appropriate.

Lastly, we create plots of the actual vs. fitted flame times as well as the average of the actual and fitted flame times (for each experiment group).
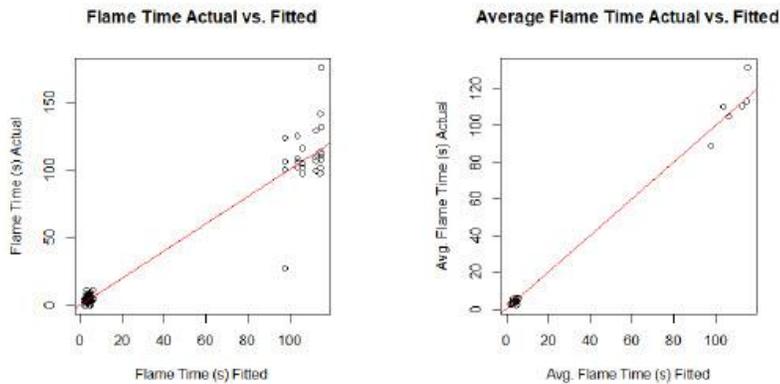
From the plots,

We see that the actual vs. fitted values follow a generally linear trend, in particular for the averages in which the variability has been removed.
This indicates that the model is performing well in predicting the actual flame time values.
These conclusions are similar to those for the zero burn length model.

Since we now have fitted values for both the burn lengths and flame times, we create a plot of the fitted burn lengths vs. fitted flame times to compare to the plot in the introduction.

Burn Length Fitted vs. Flame Time Fitted
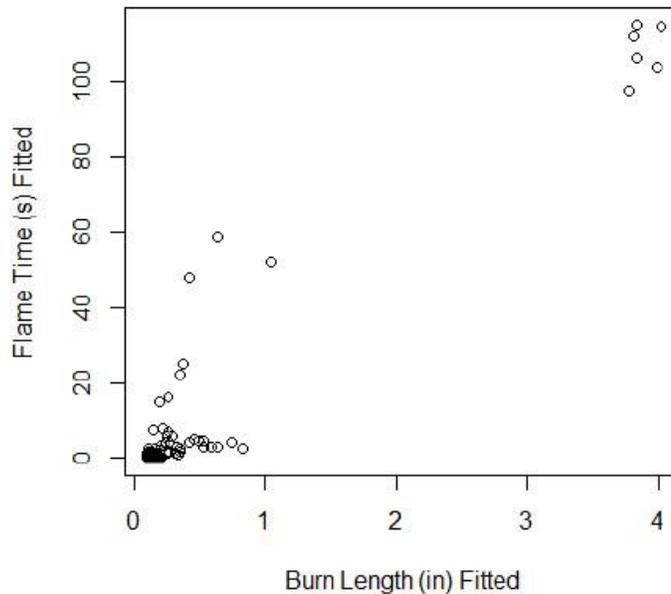
From this plot, we see that

The relationship between the fitted burn lengths and flame times are still linear, as in the plot of the actuals.

The plot of the fitted values demonstrates more separation in the data, with 6 observations having larger flame time and burn length than the remaining data.

The actual data had a few observations with long burn lengths but short flame times. Since this happened at random, the models were not able to predict these occurrences, as can be seen in the plot of the fitted values.

Dripping Model

Next we study the dripping response variable. Since dripping only occurred in 22 of the 332 observations, or about 7% of the observations, we do not fit regression models to dripping (yes/no) or drip flame time and instead look at the frequency with which dripping occurred based on the different variables.

The following is the total number of dripping and no dripping observations depending on material type.

	PEI	PEKK	PES	PEI-PC
Dripping	0	0	22	0
No Dripping	88	72	66	84
Total	88	72	88	84

From the previous table, we see that

The PES is the only material in which dripping occur.

Dripping occurred in 22 of the 88 PES observation, or about 25% of the time.

To study the occurrence of dripping in the remaining variables, we focus on only the PES material, since dripping was only observed for this material type. We begin by looking at the occurrence of dripping depending on raster width.

	0.016	0.022	0.03
Dripping	2	3	17
No Dripping	30	21	15
Total	32	24	32

From the previous table, we see that

Dripping occurred across all raster widths.

The highest rate occurred for the 0.03" raster width (the largest raster width), about 53% of the time.

We next study the occurrence of dripping depending on raster angle.

	45	90	67.5
Dripping	8	8	6
No Dripping	24	20	22
Total	32	28	28

From the previous table, we see that

Dripping occurred across the three raster angles at a similar rate.

We next study the occurrence of dripping depending on number of inner layers.

	11	4	0
Dripping	1	13	8
No Dripping	31	19	16
Total	32	32	24

From the previous table, we see that

Dripping occurred for all three inner layer values, with the highest rate occurring for 4 inner layers (41% of the time), and the least for 11 inner layers (3% of the time).

We next study the dripping depending on the infill percentage.

	60	20	0
Dripping	2	12	8
No Dripping	26	24	16
Total	28	36	24

From the previous table, we see that

Dripping occurred across all three infill percentage values.
The lowest rate (about 7%) occurring in the 60% infill percentage.

We next study the occurrence of dripping depending on the infill pattern.

	Sparse	Sparse DD	None
Dripping	8	6	8
No Dripping	20	30	16
Total	28	36	24

From the previous table, we see that

Dripping occurred across all infill patterns.
The Sparse DD pattern had the lowest rate of dripping of about 17%.
The infill pattern None (no infill) had the highest rate of dripping, with a rate of about 33%.

Therefore, we conclude that material type is the most significant predictor of dripping of these variables with dripping occurring for the levels of all other variables. These conclusions hold true even including the 100% infill percentage and the Hexagram data.

Optimization

We conclude with an analysis to find the combination of independent variables that lead to the optimal solutions for shortest burn length and smallest flame time using model fits.

Using the regression models, we predicted burn length and flame time.
We scaled the predicted values by the mean of the observed data.
For example, we scaled the prediction from the nonzero layer burn length data by the mean of the observed nonzero layer burn length observations.

We created a composite metric by multiplying these scaled values by each other: scaled flame time*scaled burn length.

This allowed us to minimize both flame time and burn length, with equal weights on both. We can sort the results by minimum or maximum values of this metric.

We calculated the composite metric for the following combinations for the main analysis:

Material (PES, PEI-PC, PEI, and PEKK)

Infill Pattern (None, Sparse, Sparse DD)

Raster Width (0.016" to 0.03", by 0.002")

Raster Angle (45° to 100°, by 7.5°)

Inner Layers (0, 4 to 11, by 1 layer)

Infill Percentage (0%, 20% to 60% by 10%)

All possible combinations in this space were considered.

Note that not all combinations were tested in the experimental design.

We evaluated the fitted models and extracted the combinations that lead to lowest composite metric.

Note that the optimization was performed on the follow-up analysis based on possible combinations in those analyses.

For the Sparse only analysis, this is: material (PES, PEI-PC, PEI, and PEKK), raster width (0.016" to 0.03", by 0.002"), raster angle (45° to 100°, by 7.5°), inner layers (4 to 11 by 1 layer), infill percentage (20% to 100% by 10%).

For the 20% only analysis, this is: material (PES, PEI-PC, PEI, and PEKK), infill pattern (Sparse, Sparse DD, and Hexagram), raster width (0.016" to 0.03", by 0.002"), raster angle (45° to 100°, by 7.5°), inner layers (4 to 11 by 1 layer).

The following table of results are provided for the main analysis, with a summary of the follow-up analysis results provided in writing.

Top 10 Combinations for Minimization

The following results provide the top 10 combinations that minimize both burn length and flame time by material type.

We begin by looking at results for PEI-PC.

Rank	Mult_Metric	Burn_Length	Flame_Time	Material	Raster_Width	Raster_Angle	Inner_Layers	Inill_Percentage	Infill_Pattern
1	0.007224	0.114910	0	PEI-PC	0.016	90.0	11	60	Sparse
2	0.008242	0.109784	0	PEI-PC	0.016	82.5	11	60	Sparse

Rank	Mult_Metric	Burn_Length	Flame_Time	Material	Raster_Width	Raster_Angle	Inner_Layers	Inill_Percentage	Infill_Pattern
3	0.008385	0.131878	0	PEI-PC	0.016	90.0	11	50	Sparse
4	0.009035	0.116086	0	PEI-PC	0.018	90.0	11	60	Sparse
5	0.009470	0.106193	0	PEI-PC	0.016	75.0	11	60	Sparse
6	0.009550	0.125922	0	PEI-PC	0.016	82.5	11	50	Sparse
7	0.009794	0.151755	0	PEI-PC	0.016	90.0	11	40	Sparse
8	0.009795	0.119916	0	PEI-PC	0.016	90.0	10	60	Sparse
9	0.010103	0.131694	0	PEI-PC	0.016	90.0	11	60	Sparse DD
10	0.010307	0.110905	0	PEI-PC	0.018	82.5	11	60	Sparse

The following table provides the top 10 combinations that minimize both burn length and flame time for the PEI material type.

Rank	Mult_Metric	Burn_Length	Flame_Time	Material	Raster_Width	Raster_Angle	Inner_Layers	Inill_Percentage	Infill_Pattern
1	0.009120	0.078621	0	PEI	0.030	90.0	11	60	Sparse DD
2	0.009540	0.076777	0	PEI	0.030	82.5	11	60	Sparse DD
3	0.010035	0.075915	0	PEI	0.030	75.0	11	60	Sparse DD
4	0.010435	0.085448	0	PEI	0.030	90.0	11	50	Sparse DD
5	0.010612	0.076005	0	PEI	0.030	67.5	11	60	Sparse DD
6	0.010911	0.083462	0	PEI	0.030	82.5	11	50	Sparse DD
7	0.011284	0.077050	0	PEI	0.030	60.0	11	60	Sparse DD
8	0.011475	0.082532	0	PEI	0.030	75.0	11	50	Sparse DD
9	0.011481	0.081147	0	PEI	0.028	90.0	11	60	Sparse DD

Ra nk	Mult_ Metric	Burn_L ength	Flame_ Time	Mat erial	Raster_ Width	Raster_ Angle	Inner_L ayers	Inill_Perc entage	Infill_P attern
10	0.0119 56	0.0928 18	0	PEI	0.030	90.0	11	40	Sparse DD

The following table provides the top 10 combinations that minimize both burn length and flame time for the PES material type.

Ra nk	Mult_ Metric	Burn_L ength	Flame_ Time	Mat erial	Raster_ Width	Raster_ Angle	Inner_L ayers	Inill_Perc entage	Infill_P attern
1	0.1139 43	0.0838 26	0.8607 25	PES	0.016	75.0	11	60	Sparse
2	0.1139 78	0.0837 37	0.8614 87	PES	0.016	82.5	11	60	Sparse
3	0.1145 54	0.0849 58	0.8599 63	PES	0.016	67.5	11	60	Sparse
4	0.1146 59	0.0846 87	0.8622 50	PES	0.016	90.0	11	60	Sparse
5	0.1158 33	0.0871 72	0.8592 01	PES	0.016	60.0	11	60	Sparse
6	0.1178 28	0.0905 46	0.8584 41	PES	0.016	52.5	11	60	Sparse
7	0.1206 13	0.0952 04	0.8576 81	PES	0.016	45.0	11	60	Sparse
8	0.1298 76	0.0870 39	0.9762 49	PES	0.016	60.0	11	60	Sparse DD
9	0.1300 01	0.0873 68	0.9753 96	PES	0.016	52.5	11	60	Sparse DD
10	0.1304 98	0.0877 86	0.9771 04	PES	0.016	67.5	11	60	Sparse DD

The following table provides the top 10 combinations that minimize both burn length and flame time for the PEKK material type.

Ra nk	Mult_ Metric	Burn_L ength	Flame_ Time	Mat erial	Raster_ Width	Raster_ Angle	Inner_L ayers	Inill_Perc entage	Infill_P attern
1	0.0145 26	0.1070 45	0.0087 41	PEKK	0.030	45.0	11	60	Sparse
2	0.0148 92	0.1041 27	0.0130 75	PEKK	0.030	52.5	11	60	Sparse
3	0.0153 65	0.1025 41	0.0175 80	PEKK	0.030	60.0	11	60	Sparse

4	0.015952	0.102225	0.022266	PEKK	0.030	67.5	11	60	Sparse
5	0.016422	0.116704	0.017455	PEKK	0.030	45.0	11	50	Sparse
6	0.016665	0.103167	0.027138	PEKK	0.030	75.0	11	60	Sparse
7	0.016789	0.113763	0.021733	PEKK	0.016	45.0	11	60	Sparse
8	0.016825	0.113511	0.022135	PEKK	0.030	52.5	11	50	Sparse
9	0.017141	0.107978	0.027739	PEKK	0.028	45.0	11	60	Sparse
10	0.017204	0.110655	0.026584	PEKK	0.016	52.5	11	60	Sparse

When looking at minimizing flame time and burn length by material type, we find that

For all materials, high inner layers and high infill percentage (40%-60%) leads to optimal conditions.
Optimal Raster Width is material dependent.
PEI-PC and PES had smaller raster widths.
PEI and PEKK had larger raster widths.
Optimal Raster Angle is material dependent.
PEI-PC and PEI had larger raster angles.
PES and PEKK had a range of raster angles, but the majority were smaller angles.
Sparse and Sparse DD infill patterns seem to lead to optimal conditions, depending on the other factors.

These conclusions also hold for the 20% infill percentage analysis, although raster width was generally small in minimizing the burn length and flame time for all the materials in this model. For the Sparse only model, these conclusions also hold except for the PEKK material type in which varying infill percentage (with high number of inner layers, large raster width, and small raster angle) minimized burn length and flame time rather than a higher infill percentage as was found for the remaining results.

Top 10 Combinations for Maximization

The following results provide the top 10 combinations that maximize both burn length and flame time by material type.

We begin by looking at results for PEI-PC.

Ra nk	Mult_ Metric	Burn_L ength	Flame_ Time	Mat erial	Raster_ Width	Raster_ Angle	Inner_L ayers	Inill_Perc entage	Infill_P attern
1	2.9001 27	0.9033 48	4.3800 50	PEI-PC	0.016	90.0	0	0	None
2	2.3821 81	0.7339 49	4.3274 38	PEI-PC	0.016	45.0	0	0	None
3	2.2068 65	0.8740 27	3.4117 35	PEI-PC	0.016	82.5	0	0	None
4	2.2056 06	0.7933 60	3.7266 50	PEI-PC	0.018	90.0	0	0	None
5	2.0880 22	0.5632 32	4.7796 31	PEI-PC	0.030	45.0	0	0	None
6	1.9337 28	0.7610 95	3.3806 59	PEI-PC	0.016	52.5	0	0	None
7	1.8754 07	0.4890 31	4.8348 57	PEI-PC	0.030	90.0	0	0	None
8	1.8707 18	0.6674 66	3.6780 37	PEI-PC	0.018	45.0	0	0	None
9	1.8198 55	0.8451 42	2.8843 99	PEI-PC	0.016	75.0	0	0	None
10	1.7822 67	0.7034 65	3.3381 37	PEI-PC	0.020	90.0	0	0	None

The following table provides the top 10 combinations that maximize both burn length and flame time for the PEI material type.

Ra nk	Mult_ Metric	Burn_L ength	Flame_ Time	Mat erial	Raster_ Width	Raster_ Angle	Inner_L ayers	Inill_Perc entage	Infill_P attern
1	2.0098 34	0.5299 79	4.8448 27	PEI	0.030	45.0	0	0	None
2	1.7993 03	0.4577 19	4.9004 19	PEI	0.030	90.0	0	0	None
3	1.5704 37	0.5176 30	3.8410 24	PEI	0.030	52.5	0	0	None
4	1.5106 39	0.4154 43	4.4425 28	PEI	0.016	90.0	0	0	None
5	1.4892 82	0.4583 24	4.0343 57	PEI	0.028	45.0	0	0	None
6	1.4600 94	0.4694 56	3.8740 88	PEI	0.030	82.5	0	0	None

Rank	Mult_Metric	Burn_Length	Flame_Time	Material	Raster_Width	Raster_Angle	Inner_Layers	Inill_Percentage	Infill_Pattern
7	1.398406	0.417886	4.085203	PEI	0.028	90.0	0	0	None
8	1.326624	0.505404	3.296410	PEI	0.030	60.0	0	0	None
9	1.279593	0.481317	3.311742	PEI	0.030	75.0	0	0	None
10	1.235957	0.493299	3.128843	PEI	0.030	67.5	0	0	None

The following table provides the top 10 combinations that maximize both burn length and flame time for the PES material type.

Rank	Mult_Metric	Burn_Length	Flame_Time	Material	Raster_Width	Raster_Angle	Inner_Layers	Inill_Percentage	Infill_Pattern
1	311.0186	4.171934	112.7441	PES	0.016	90.0	0	0	None
2	305.2791	4.021115	114.7153	PES	0.030	45.0	0	0	None
3	292.7502	4.111203	107.6478	PES	0.016	82.5	0	0	None
4	292.0126	3.832868	114.9825	PES	0.030	90.0	0	0	None
5	291.5641	4.028480	109.3614	PES	0.018	90.0	0	0	None
6	289.5973	3.989435	109.6611	PES	0.030	52.5	0	0	None
7	285.7669	3.898538	110.6715	PES	0.028	45.0	0	0	None
8	284.2960	3.814072	112.4795	PES	0.016	45.0	0	0	None
9	281.1556	3.863937	109.8353	PES	0.030	82.5	0	0	None
10	280.4753	4.050907	104.6294	PES	0.016	75.0	0	0	None

The following table provides the top 10 combinations that maximize both burn length and flame time for the PEKK material type.

Rank	Mult_Metric	Burn_Length	Flame_Time	Material	Raster_Width	Raster_Angle	Inner_Layers	Inill_Percentage	Infill_Pattern

1	1.831308	0.396477	5.617154	PEKK	0.016	90.0	0	0	None
2	1.566013	0.293557	6.067439	PEKK	0.030	45.0	0	0	None
3	1.417250	0.375916	4.515651	PEKK	0.016	82.5	0	0	None
4	1.414662	0.340673	4.875696	PEKK	0.018	90.0	0	0	None
5	1.385769	0.279637	5.557700	PEKK	0.016	45.0	0	0	None
6	1.354075	0.236904	6.129507	PEKK	0.030	90.0	0	0	None
7	1.247978	0.283809	4.939745	PEKK	0.030	52.5	0	0	None
8	1.232296	0.263250	5.158069	PEKK	0.028	45.0	0	0	None
9	1.178610	0.355791	3.907946	PEKK	0.016	75.0	0	0	None
10	1.176137	0.298023	4.480014	PEKK	0.016	52.5	0	0	None

When looking at maximizing flame time and burn length by material type, we find that

Zero inner layers (0% infill percentage) maximized flame time and burn length for all materials. The raster widths and raster angles varied.

Therefore, for all materials, the zero inner layers maximized burn length and flame time, with different combinations of raster angle and raster width.

These conclusions also hold for the 20% infill percentage analysis. In particular, the smallest number of inner layers maximized burn length and flame time, with different combinations of the raster angle and raster width. For the Sparse only model, these conclusions also hold except for the PEKK material type in which high infill percentage (along with a small number of inner layers, small raster width and large raster angle) maximized burn length and flame time rather than a low infill percentage as was found for the remaining results.

Conclusions

In summary, the regression models show that material, raster width, raster angle, inner layers, infill percentage, and infill pattern are all significant as either main or interaction effects in predicting the burn length. All the factors except infill pattern are also significant in predicting flame time. In particular, material is a very significant main effect variable in predicting both

burn length and flame time for nonzero and zero layer data. Inner layer and infill percentage are also significant main effect variables in predicting both burn length and flame time for the nonzero layer data. Although raster width and raster angle are less significant as main effect variables, they are significant as interaction effect variables with other variables. Therefore, all variables are significant in predicting the burn length, and all but infill pattern are significant in predicting the flame time.

The occurrence of dripping is less related to the independent variables, although material type (specifically, PES) is the most significant variable in driving the variability in the occurrence of dripping. From the original data, we find that dripping only occurred for the PES material, although it occurred in most observations of the other variables.

We found that burn length and flame time are minimized with PEI-PC or PEI material, small raster width, large raster angles, high number of inner layers, high infill percentage, and with Sparse or Sparse DD pattern. In general, a high number of inner layers and infill percentage as well as Sparse or Sparse DD patterns minimized both burn length and flame time. The raster widths and raster angles depended on the material type. We also found that PES material with no inner layers maximized flame time and burn length. In general, no inner layers maximized flame time for all materials, with raster widths and raster angles varying by material. These conclusions generally held true for the follow-up analyses, except for the PEKK material in the Sparse only model in which the infill percentage conclusions varied. As a confirmatory analysis to the minimization/maximization results presented, we suggest completing some testing on the top combinations that were found to provide the minimum and maximum burn lengths and flame times to ensure that the model results are confirmed with real experimental data (as not all combinations were completed as part of the design of experiment).